Accepted Manuscript

Design and synthesis novel di-carbonyl analogs of curcumin (DACs) act as potent anti-inflammatory agents against LPS-induced acute lung injury (ALI)

Jianchang Qian, Xianxin Chen, Sheng Shu, Wenxin Zhang, Bo Fang, Xiaojing Chen, Yunjie Zhao, Zhiguo Liu, Guang Liang

PII: S0223-5234(19)30156-4

DOI: https://doi.org/10.1016/j.ejmech.2019.02.042

Reference: EJMECH 11134

To appear in: *European Journal of Medicinal Chemistry*

Received Date: 1 November 2018

Revised Date: 11 February 2019

Accepted Date: 11 February 2019

Please cite this article as: J. Qian, X. Chen, S. Shu, W. Zhang, B. Fang, X. Chen, Y. Zhao, Z. Liu, G. Liang, Design and synthesis novel di-carbonyl analogs of curcumin (DACs) act as potent anti-inflammatory agents against LPS-induced acute lung injury (ALI), *European Journal of Medicinal Chemistry* (2019), doi: https://doi.org/10.1016/j.ejmech.2019.02.042.

Design and synthesis novel di-carbonyl analogs of curcumin (DACs) act as potent anti-inflammatory agents against LPS-induced acute lung injury (ALI)

Jianchang Qian [1,#], Xianxin Chen [1,#], Sheng Shu [1,#], Wenxin Zhang [1], Bo Fang [1], Xiaojing Chen [1], Yunjie Zhao [1,*], Zhiguo Liu [1,*], Guang Liang [1]

[1] Chemical Biology Research Center at School of Pharmaceutical Sciences, Wenzhou Medical University, 1210 University Town, Wenzhou, Zhejiang 325035, China

Graphical abstract:

Novel di-carbonyl analogs of curcumin (DACs) were designed, synthesized and evaluated for anti-inflammatory activities for the treatment of ALI.

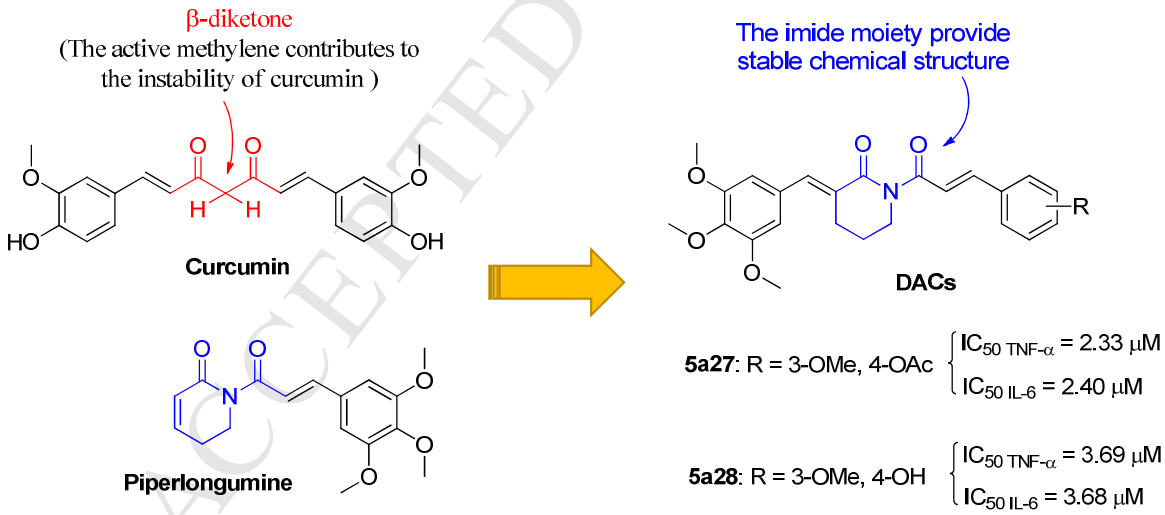

Design and synthesis novel di-carbonyl analogs of curcumin (DACs) act as potent anti-inflammatory agents against LPS-induced acute lung injury (ALI)

Jianchang Qian [1,#], Xianxin Chen [1,#], Sheng Shu [1,#], Wenxin Zhang [1], Bo Fang [1], Xiaojing Chen [1], Yunjie Zhao [1,*], Zhiguo Liu [1,*], Guang Liang [1]

[1] Chemical Biology Research Center at School of Pharmaceutical Sciences, Wenzhou Medical University, 1210 University Town, Wenzhou, Zhejiang 325035, China

[#] These authors contribute equally to this work.

* Corresponding author:
Yunjie Zhao, Ph.D, Associate Professor
Chemical Biology Research Center at School of Pharmaceutical Sciences, Wenzhou Medical University. 1210 University Town, Wenzhou, Zhejiang 325035, China
Tel: (+86)-577-86699892; Fax: (+86)-577-86699892
E-mail: aabye1100@aliyun.com

and Zhiguo Liu, Ph.D, Associate Professor
Chemical Biology Research Center at School of Pharmaceutical Sciences, Wenzhou Medical University. 1210 University Town, Wenzhou, Zhejiang 325035, China
Tel: (+86)-577-86699892; Fax: (+86)-577-86699892
E-mail: lzgcnu@163.com

Abstract

A novel series of di-carbonyl analogs of curcumin (DACs) were prepared and evaluated for their anti-inflammatory properties. Preliminary results showed that a vast majority of compounds tested in this study could effectively suppress LPS-induced overproduction of tumor necrosis factor (TNF)-α and interleukin (IL)-6. Structure-activity relationships of the compounds were discussed. Compounds **5a27** and **5a28** showed the most potent anti-inflammatory activities and had higher structural stability and orally bioavailability than curcumin *in vitro*. Mechanistically, they inhibited the activation of macrophages via the blockade of mitogen-activated protein kinase (MAPK) signaling and nuclear translocation of NF-κB. *In vivo*, **5a27** and **5a28** markedly alleviated lipopolysaccharides (LPS)-induced acute lung injury (ALI). The wet/dry ratio of lungs was significantly normalized by the active compounds, which was consistent with the suppression of neutrophil infiltration and production of proinflammatory cytokines. Collectively, these results present a new series of curcumin analogs as promising anti-inflammatory agents for treatment of ALI.

Key words: Di-carbonyl analogs of curcumin; Structural stability; Acute lung injury; Anti-inflammation.

1. Introduction

Acute lung injury (ALI) is a severe clinical syndrome of hypoxemic respiratory failure with substantial morbidity and mortality [1]. Even survivors of ALI have their long-term quality of life compromised owing to a lack of effective therapeutic approaches [2, 3]. Recent advances in unveiling the pathogenesis of ALI have identified the blockade of excessively inflammatory cascades as an effective strategy to attenuate lung injury [4]. Despite some encouraging preclinical evidence for potential pharmacological treatments, the phase III clinical trials of most of the drug candidates, such as glucocorticoids, surfactants and procysteine, were not successful. There is thus an unmet need for effective anti-inflammatory drugs to treat patients with ALI [5].

Bacterial infection is one of the most common causes of ALI [6]. Release of endotoxins, especially lipopolysaccharide (LPS), is the leading contributor. This is a potent activator of toll-like receptor 4 (TLR4), which triggers the nuclear translocation of the nuclear factor κB (NF-κB), thereby promoting the transduction of proinflammatory molecules, such as cytokines interleukin 6 (IL-6), IL-1β and tumor necrosis factor α (TNF-α) [7]. Therefore, suppression of inflammatory responses by blocking activation of NF-κB could be a potential strategy of treating ALI.

Natural products and their plant-derived analogs are expected to play a crucial role in the design of novel anti-inflammatory agents [8, 9]. Curcumin, [(1,7-bis(4-hydroxy-3-methoxyphenyl)-1,6-heptadiene-3,5-dione)], is a phenolic compound originally isolated from the rhizome of *Curcuma longa*. Its anti-inflammatory [10-12], antioxidant [13] and antitumor activities [14, 15] have attracted much attention along with its favorable toxicity profile. However, the clinical development of curcumin is limited by its instability and poor solubility in water, resulting in limited oral bioavailability which fails to reach the minimum effective therapeutic concentration [16, 17]. Previous studies have demonstrated that the active methylene group of the β-diketone moiety in the structure of curcumin could be related to its instability under physiological conditions, inducing rapid degradation and metabolism [18-20]. In another study, curcumin was incubated in buffer solutions of pH 7.2 at 37 °C, and about 90% degraded within 30 min. *Trans*-6-(4'-hydroxy-3'-methoxyphenyl)-2,4-dioxo-5-hexenal was

predicted as the key degradation product and vanillin, ferulic acid and feruloyl methane were identified as minor degradation products [21] (Fig. 1). Numerous curcumin analogs have been designed and synthesized in an attempt to overcome these limitations and improve the chemical instability.

Recently, our research group has synthesized a panel of mono-carbonyl analogues of curcumin (MACs), by modifying the central β-diketone moiety to a mono ketone group. These MACs exhibited greater metabolic stability and bioactivity than the parent molecule [22, 23]. For example, we incorporated the active methylene group into an α, β-unsaturated cyclohexanone, and changed the substituted benzene rings into 3,4,5-trimethoxyphenyl rings, to furnish a structurally symmetrical MAC **C03**. Pleasingly, a higher anti-inflammatory activity and stability were observed with **C03** than that of curcumin. Additionally, in our ongoing search for similar functional groups that are able to replace the unstable β-diketone moiety in curcumin, we investigated a new chemical entity containing an imide moiety. Isolated from the plant long pepper (Piper longum), piperlongumine (PL) constitutes two α, β-unsaturated imides and exhibits highly selective anticancer activities and remarkable anti-inflammatory properties [24, 25]. Interestingly, the structure of PL also contains an active 3,4,5-trimethoxyphenyl group. Encouraged by these findings, we introduced piperidin-2-one and 3,4,5-trimethoxyphenyl moieties into the curcumin skeleton to afford a series of novel di-carbonyl analogs of curcumin (DACs) whose biological activities were then evaluated.

Please insert the Figure 1

2. Results and discussion

2.1. Chemistry

The syntheses and structures of the DACs (**6a01–6a29**) are illustrated in Scheme 1. Briefly, treatment of commercially available or previously synthesized cinnamic acids (**1a01–24, 1a26–27, 1a29**) with oxalyl chloride and a catalytic amount of DMF provided the corresponding cinnamoyl

chlorides **2a01–24**, **2a26–27** and **2a29**. After simple work-up to remove most of the solvent, the crude products were used directly for the next step without further purification. Alternatively, the other key intermediate (*E*)-3-(3,4,5-trimethoxybenzylidene) piperidin-2-one (**4**) was prepared from commercially available 3,4,5-trimethoxybenzaldehyde (**3**) with *tert*-butyl 2-oxopiperidine-1-carboxylate in the presence of sodium hydride. The title amides **5a01–5a24**, **5a26–5a27** and **5a29** were furnished in satisfactory yields via coupling of intermediate **4** and the previously synthesized cinnamoyl chlorides. Furthermore, after catalytic removal of the acetyl protecting group in 20% $NaHCO_3$, **5a24** and **5a27** were successfully converted into desired compounds **5a25** and **5a28**, respectively. The structures of all new DACs were fully characterized by proton nuclear magnetic resonance (^{1}H NMR), carbon nuclear magnetic resonance (^{13}C NMR) and electrospray ionization mass spectrometry (ESI-MS).

Please insert the Scheme 1

2.2 Structure-activity relationship (SAR) and cytotoxic evaluation

Lipopolysaccharide (LPS) is a major biologically active component of Gram-negative bacteria and plays an important role in the development of systemic inflammation responses, especially in the expression of several inflammatory cytokines, such as TNF-α and IL-6 [26, 27]. Furthermore, these two cytokines activate an inflammatory-induced ALI reaction process [28]. To explore the inhibitory effects of the new DACs, LPS induced production of TNF-α and IL-6 was determined in mouse primary macrophages (MPMs). Following an established procedure [29], all the newly synthesized compounds were tested for *in vitro* anti-inflammatory activity through an enzyme-linked immunosorbant assay (ELISA) at a single concentration of 10 μM (Fig.2A and B).

Our initial biological screening indicated that the majority of DACs exhibited effective inhibition (39.6–99.5% inhibitory rates) against the LPS-stimulated production of both TNF-α and IL-6. Compounds **5a01–5a07**, with mono-halogen substituents in the phenyl ring, had weak potency in inhibiting release of either IL-6 or TNF-α (inhibitory rates <85.3%), relative to the

positive control of curcumin or PL. However, the DAC **5a08** with a strong electron-withdrawing nitro group at the *para*-position of the phenyl ring, demonstrated marked inhibitory activities (94.1% and 38.6% for IL-6 and TNF-α, respectively). For further enhancement of anti-inflammatory activity, di-substituted compounds **5a09–5a16**, bearing di-halogens or 2-fluoro atoms at the phenyl ring, were evaluated. 3,4-Difluoro, 2,6-dichloro and 2-fluoro-4-methoxy substituted compounds **5a09**, **5a12** and **5a16**, showed comparable *in vitro* activities to that of curcumin. Conversely, introduction of 2,5-difluoro (**5a10**), 2,4-dichloro (**5a11**), 2-fluoro-6-chloro (**5a13**), 2-chloro-4-fluoro (**5a14**) and 2-fluoro-5-methoxy (**5a15**) substituents to the phenyl ring afforded significantly reduced potencies, with inhibition rates ranging from 38.5% to 53.4% (for TNF-α) and 46.8% to 68.2% (for IL-6).

Incorporation of a methoxy group at different positions of the phenyl ring yielded compounds **5a17–5a22**. Except compound **5a20**, which had a 2,3-dimethoxyphenyl ring, these compounds exhibited significant inhibition on the production of IL-6 and TNF-α. Changing from the two fluoro groups in **5a10** to the methyl groups in **5a23** gave a similar potency with slightly increased inhibition of TNF-α production. With the phenyl ring in place, we next incorporated hydroxy groups or acetoxy groups at the *ortho*-, *meta*- or *para*- position, yielding compounds **5a24–5a29** which provided higher IL-6 inhibition than that of curcumin. Notably, greater activity occurred when the methoxy group was located at the *meta*-position (**5a18**, **5a22**, **5a27** and **5a28**), indicating that the position of the methoxy group might play an important role in the activity. Importantly, compounds **5a27** and **5a28** with a hydroxyl or acetoxy substituent at the *para*- position of the phenyl ring displayed the greatest effects in reducing LPS-induced TNF-α and IL-6 production, with their inhibitory rates reaching 90.9–92.5% (for TNF-α) and 99.3–99.7% (for IL-6), respectively. These findings support the anti-inflammatory effects of the novel di-carbonyl analogs of curcumin.

Please insert the Figure 2

Before further studies, the cytotoxicity and safety of these synthetic DACs were evaluated in

MPMs by MTT assays at concentration of 10 μM. As shown in Fig. 2C, almost all of the compounds exhibited no significant effects on cell proliferation, supporting their reasonable safety. What's more, no significant differences were observed while comparing DACs to PL and curcumin.

2.3 Dose-dependent inhibition of LPS-induced release of cytokines

DACs effectively inhibited the production of proinflammatory cytokines without significant cytotoxicity. To further investigate the anti-inflammatory activities of the active compounds, two of the most potent compounds, **5a27** and **5a28**, were selected. As shown in Fig.3A and B, **5a27** and **5a28** exhibited dose-dependent inhibition of LPS-induced release of TNF-α and IL-6 in active RAW 264.7 mouse macrophages, within the dose range of 2.5 to 20 μM. The potency of DACs in suppressing TNF-α and IL-6 production is much higher than curcumin's. The IC_{50} values of **5a27** and **5a28** were at the low μM levels (**5a27:** 2.33 ± 0.78 μM and 2.40 ± 0.44 μM for TNF-α and IL-6 respectively; **5a28:** 3.69 ± 1.34 μM and 3.68 ± 0.59 μM for TNF-α and IL-6 respectively), rendering these compounds promising anti-inflammatory agents.

Please insert the Figure 3

2.4 Chemical stability and orally bioavailability

In view of the limited clinical application of curcumin resulting from its instability and poor metabolism, we designed and synthesized these chemically modified DACs. Among them, the most active analogs **5a27** and **5a28** were chosen for stability test in phosphate buffer (pH 7.4) using ultraviolet-visible (UV-visible) spectroscopy. As shown in Fig. 4A, the optical density (OD) values of the maximal absorption peak of curcumin decreased quickly within 25 min, consistent with those of previous reports. Of interest, the two DACs **5a27** and **5a28** only slightly decomposed during incubation, demonstrating remarkable structural stability under the same condition (Fig.4B and C). This result suggests that these modified active DACs are chemically more stable than curcumin *in vitro*.

Poor bioavailability is another dramatical problem that hinder the application of curcumin. Therefore, the most active DAC, **5a27**, was chosen to determine the orally bioavailability. As Fig. 4D shown, there were two absorption peaks after intragastric administration. So, it's probably following liver and intestinal circulation. The pharmacokinetic parameters were determined and shown in Table 1. According to formula $F = \frac{AUC\ p.o \times Dose\ i.v}{AUC\ i.v \times Dose\ p.o}$, orally bioavailability of **5a27** was figured out, which is 26.62 %. However, the bioavailability of curcumin was reported to be 1 % previously [30]. The data proved that the bioavailability of DACs was dramatically improved compared to Curcumin.

Please insert the Figure 4 and Table 1

2.5 Mechanism of suppression of inflammatory responses

Having shown that **5a27** and **5a28** potently inhibited LPS-induced macrophage activation and presented higher stability than curcumin, we explored the underlying mechanism of the anti-inflammatory effects by studying the MAPK signal pathway. Mitogen-activated protein kinases (MAPKs), a family of serine/threonine protein kinases, are widely known to mediate fundamental biological processes of inflammatory responses [31]. By activation of the MAPK signaling pathway, especially p38 and ERK, inflammation mediators can be regulated at the transcription and translation levels. Thus, the MAPK signaling pathway carries potential targets for anti-inflammatory therapeutics. Furthermore, that the pathway has been recognized as the mechanistic target of curcumin lends further support to the notion. Therefore, we evaluated the effects of **5a27** and **5a28** on the MAPK signaling pathway. RAW 264.7 mouse macrophages were pretreated with the compounds for half of an hour, followed by stimulation with LPS for 30 minutes. The cell lysates were harvested and immunoblotted. As shown in Fig. 5A, **5a27** and **5a28** markedly inhibited P-P38 and P-ERK, indicating the suppression of MAPK signaling. However, the potency of inhibiting P-P38 by **5a28** was lower compared to **5a27** and curcumin.

Nuclear factor κB (NF-κB) is a protein complex that controls the transcription of cytokines, e.g. TNF-α and ILs, and is regulated downstream by MAPK. Consistent with the inhibition of

MAPK signaling cascades, IκB (inhibitor of NF-κB) was significantly down-regulated by **5a27** and **5a28** (Fig.5A). Meanwhile, the translocation of P65, a component of NF-κB activation, was significantly attenuated by treatment with the active compounds (Fig. 5B). Given that inactivation of NF-κB would block transcription of proinflammatory cytokines, we further determined the effects of the active DACs on the RNA level of proinflammatory factors. As shown in Fig. 5C–G, **5a27** and **5a28** significantly inhibited the transcription of TNF-α, IL-6, IL-1β, ICAM-1 and VCAM-1 compared with LPS alone. These data solidly indicated that **5a27** and **5a28** potently inhibited inflammation through blocking MAPK signal transduction and inactivation of NF-κB.

Please insert the Figure 5

2.6 Alleviation of LPS-induced acute lung injury

The active compounds were evaluated in a ALI mouse model over a week. Thus **5a27**, **56a28** and curcumin were administered to C57/BL6 mice at 10 mg/kg intraperitoneally and sacrificed 6 hours later. ALI is characterized by rapid-onset respiratory failure following direct and indirect insults to the lung parenchyma and vasculature. We therefore investigated the wet/dry weight ratio of the mice lungs, which was dramatically increased by LPS and significantly reduced by **5a27** and **5a28** (Fig. 6A). These results indicated that cell infiltration in lung tissues was suppressed after treatment with the DACs. Examination of bronchoalveolar lavage fluid (BALF) revealed that the DACs normalized total cell count and neutrophil count in BALF (Fig. 6B-C). Histological evaluation of the mice lungs revealed typical histopathological alterations in ALI. In the LPS group, interstitial edema, pulmonary congestion, thickened alveolar septa, inflammatory infiltration and lung tissue destruction were observed (Fig. 6D). **5a27** and **5a28** however, dramatically improved the pathological lesions compared with the LPS group. Besides, positive staining of biomarkers of lymphocytes and macrophages was significantly attenuated after treatment (Fig.6D).

Please insert the Figure 6

Proinflammatory factors, TNF-α and IL-6 play a critical role in driving inflammation in the early phase of ALI. As shown in Fig. 6E–H, release of TNF-α and IL-6 was obviously inhibited compared with the LPS group either in serum or BALF. Moreover, challenge of LPS increased the mRNA expression of inflammatory cytokines and adhesion factors, such as TNF-α, IL-6, IL-1β, VACM-1 and ICAM-1. However, their expressions were markedly suppressed after treatment with DACs (Fig.7 A–E). Collectively, these results indicated that **5a27** and **5a28** could potently protect against pulmonary inflammation *in vivo*, and this novel chemical scaffold could potentially be used for treating ALI and other inflammatory injures.

Please insert the Figure 7

3. Conclusion

In summary, we have synthesized a series di-carbonyl analogs of curcumin (DACs) and their anti-inflammatory activity was evaluated. The majority of synthetic DACs were effective in inhibiting LPS-induced production of TNF-α and IL-6 in MPMs. Key preliminary SAR findings included that 1) mono-halogen substituent in the phenyl ring decreased the anti-inflammation, but a strong electron-withdrawing (such as nitro group) at the *para*-position of the phenyl ring, resulted in a significant increase in activities; 2) The position and number of methoxy group in phenyl ring was crucial for the inhibitory activity. The most potent DACs **5a27** and **5a28** showed higher chemical stability than curcumin in the biological medium. Mechanistical study found that DACs significantly inhibit inflammation via blocking MAPK signaling pathway and activation of NF-κB. Furthermore, pretreatment with these two active compounds attenuated LPS-induced ALI in mice via reducing the production of inflammatory cytokines, the W/D ratio, and inflammatory cell infiltration into lung tissue. Overall, this study supports the notion that anti-inflammatory DACs could be a promising strategy for the treatment of ALI. Continued medicinal chemistry

efforts should be made to obtain potent and drug-like DACs for potential use in clinic.

4. Experimental

4.1 General methods

All reagents and solvents of analytical grade were purchased from local suppliers and were used without further purification while following special instructions. All reactions were performed in a dry nitrogen atmosphere unless otherwise noted. The progress of reactions was monitored by silica gel thin layer chromatography (250 μ silica gel 60 F_{254} glass plates) and the spots were detected under UV light (254 nm). Column chromatography was performed using Merck silica gel 60 (200–300 mesh ASTM) (Merck KGaA, Darmstadt, Germany). ^{1}H and ^{13}C NMR spectra were recorded by a Bruker instrument (Brucker AVANCE DRX-500) with tetramethylsilane (TMS) as an internal standard (500 MHz for ^{1}H, 125 MHz for ^{13}C). The ^{1}H or ^{13}C NMR spectra of target anti-inflammatory compounds were provided in the Supplementary data. Melting points were obtained on a Fisher-Johns melting apparatus and were uncorrected. Electron-spray ionization mass spectroscopy (ESI-MS) data were collected in positive mode using a Bruker Esquire 3000t spectrometer.

4.2 General procedures for the synthesis of cinnamoyl chlorides (2a01-24, 2a26-27, 2a29)

To a solution of cinnamic acid (**1a01-24, 1a26-27, 1a29**) (1.0 mmol) in dry CH_2Cl_2 was added oxalyl chloride (5.0 equiv) and a catalytic amount of DMF (0.01 equiv). The reaction mixture was stirred at room temperature for 5 h before the solvent was removed. The residue was dried under high vacuum and used in the next step without further purification**.**

4.2 Synthesis of (*E*)-3-(3,4,5-trimethoxybenzylidene)piperidin-2-one (4)

A solution of NaH (0.376 g, 12.55 mmol) in dry THF (2 mL) was stirred at 0 °C for 10 min, and then a solution of *tert*-butyl 2-oxopiperidine-1-carboxylate (0.50 g, 2.51 mmol) and 3,4,5-trimethoxybenzaldehyde **(3)** (0.54 g, 2.76 mmol) in dry THF (2 mL) was added slowly. The reaction mixture was stirred at room temperature for 4 h. The resulting solution was then

quenched with saturated NH_4Cl solution (40 mL) and extracted with EtOAc (3×50 mL). The combined organic layers were washed with water (100 mL), brine (100 mL), dried over anhydrous $MgSO_4$, filtered and concentrated *in vacuo*. The residue was purified by column chromatography on silica gel providing the desired compound **4** (0.20 g, 28.7%) as a white powder. ^{1}H NMR (500 MHz, $CDCl_3$) δ (ppm): 7.72 (s, 1H), 6.89 (s, 1H), 6.62 (s, 2H), 3.85 (s, 10H), 3.43 (s, 2H), 2.83 (t, *J* = 5.5 Hz, 2H), 1.95 – 1.80 (m, 2H).

4.3 General procedures for the synthesis of DACs 5a01–5a29

A 1.6 M solution of *n*-BuLi in hexane (0.26 mL, 0.43 mmol) was added dropwise to a solution of (*E*)-3-(3,4,5-trimethoxybenzylidene)piperidin-2-one (**4**) (0.36 mmol) in anhydrous THF (4 mL) at −78 °C under nitrogen. After 2 h, a solution of cinnamoyl chlorides (**2a01–24, 2a26–27, 2a29**) (1.0 mmol) in dry THF (2 mL) wad added dropwise. The reaction solution was stirred for 10 min and then allowed to warm up to room temperature for 2 h. The resulting mixture was quenched with saturated NH_4Cl solution (10 mL), and the mixture was extracted with AcOEt (3×25 mL). The organic layers were dried over $MgSO_4$ and concentrated at reduced pressure. The residue was purified by column chromatography on silica gel providing the target compounds **5a01–5a29**.

4.3.1 (*E*)-1-[(*E*)-3-(2-Fluorophenyl)acryloyl]-3-(3,4,5-trimethoxybenzylidene)piperidin-2-one (5a01).

Yellow powder, 36.3% yield, m.p: 135.8-138.3 °C. ^{1}H NMR (500 MHz, $CDCl_3$) δ (ppm): 7.86 (d, *J* = 16.1 Hz, 2H), 7.68 – 7.63 (m, 2H), 7.34 (dd, *J* = 13.3, 6.8 Hz, 1H), 7.15 (t, *J* = 7.5 Hz, 1H), 7.12 – 7.06 (m, 1H), 6.69 (s, 2H), 3.92 – 3.89 (m, 11H), 2.90 (t, *J* = 5.6 Hz, 2H), 2.00 – 1.94 (m, 2H). ^{13}C NMR (125 MHz, $CDCl_3$) δ (ppm): 169.7, 167.8, 153.1, 139.5, 139.0, 135.1, 131.2, 130.8, 129.6, 128.9, 124.7, 124.2, 116.1, 115.9, 107.7, 60.9, 56.2, 44.1, 26.4, 22.4. ESI-MS m/z: 426.26 $(M)^+$.

4.3.2 (*E*)-1-[(*E*)-3-(3-Fluorophenyl)acryloyl)]-3-(3,4,5-trimethoxybenzylidene)piperidin-2-one (5a02). Yellow powder, 38.7% yield, m.p: 97.1-98.0 °C. ^{1}H NMR (500 MHz, $CDCl_3$) δ (ppm): 7.87 (s, 1H), 7.65 (d, *J* = 15.52 Hz, 1H), 7.58 (d, *J* = 15.58 Hz, 1H), 7.35 (s, 1H), 7.34 (d, *J* =

11.32 Hz, 1H), 7.30 (d, *J* = 10.06 Hz, 1H), 7.06 (t, *J* = 6.29 Hz, 1H), 6.69 (s, 2H), 3.93-3.91 (m, 2H), 3.89 (s, 3H), 3.88 (s, 6H), 2.93 – 2.88 (m, 2H), 2.01 – 1.94 (m, 2H). ^{13}C NMR (125 MHz, $CDCl_3$) δ (ppm): 169.5, 167.9, 153.1, 141.3, 139.6, 130.8, 130.2, 130.2, 129.6, 124.2, 123.8, 116.7, 116.6, 114.4, 114.2, 107.9, 60.9, 56.2, 44.0, 26.4, 22.4. ESI-MS m/z: 426.13 $(M)^+$.

4.3.3 (*E*)-1-[(*E*)-3-(4-Fluorophenyl)acryloyl]-3-(3,4,5-trimethoxybenzylidene)piperidin-2-one (5a03).

Yellow powder, 38.5% yield, m.p: 131.4-133.1 °C. ^{1}H NMR (500 MHz, $CDCl_3$) δ (ppm): 7.87 (s, 1H), 7.69 (d, *J* = 15.6 Hz, 1H), 7.59 (dd, *J* = 8.3, 5.6 Hz, 2H), 7.54 (d, *J* = 15.6 Hz, 1H), 7.07 (t, *J* = 8.5 Hz, 2H), 6.69 (s, 2H), 3.92 – 3.89 (m, 11H), 2.90 (t, *J* = 5.7 Hz, 2H), 2.00 – 1.94 (m, 2H). ^{13}C NMR (125 MHz, $CDCl_3$) δ (ppm): 169.7, 167.9, 153.1, 141.7, 139.5, 139.1, 130.8, 130.1, 129.7, 122.1, 115.9, 115.7, 107.7, 60.9, 56.2, 44.0, 26.4, 22.4. ESI-MS m/z: 426.19 $(M)^+$.

4.3.4 (*E*)-1-[(*E*)-3-(2-Chlorophenyl)acryloyl]-3-(3,4,5-trimethoxybenzylidene)piperidin-2-one (5a04).

Yellow powder, 41.5% yield, m.p: 134.1-135.7 °C. ^{1}H NMR (500 MHz, $CDCl_3$) δ (ppm): 8.10 (d, *J* = 15.6 Hz, 1H), 7.86 (s, 1H), 7.74 (d, *J* = 7.00 Hz, 1H), 7.58 (d, *J* = 15.5 Hz, 1H), 7.40 (d, *J* = 7.19 Hz, 1H), 7.30 – 7.27 (m, 2H), 6.68 (s, 2H), 3.92 (t, *J* = 5.82 Hz, 2H), 3.89 (s, 3H), 3.88 (s, 6H), 2.90 (t, *J* = 5.67 Hz, 2H), 1.99 – 1.94 (m, 2H). ^{13}C NMR (125 MHz, CDCl3) δ (ppm): 169.4, 167.9, 153.1, 139.6, 139.1, 138.4, 135.0, 133.5, 130.8, 130.6, 130.0, 129.6, 127.9, 126.9, 124.9, 107.7, 60.9, 56.2, 44.0, 26.4, 22.4. ESI-MS m/z: 442.29 $(M)^+$.

4.3.5 (*E*)-1-[(*E*)-3-(3-Bromophenyl)acryloyl]-3-(3,4,5-trimethoxybenzylidene)piperidin-2-one (5a05).

Yellow powder, 42.3% yield, m.p: 113.8-116.4 °C.^{1}H NMR (500 MHz, $CDCl_3$) δ (ppm): 7.87 (s, 1H), 7.75 (s, 1H), 7.62 (d, *J* = 15.61 Hz, 1H), 7.57 (d, *J* = 15.61 Hz, 1H), 7.49 (t, *J* = 7.66 Hz, 2H), 7.24 (d, *J* = 7.81 Hz, 1H), 6.99 (s, 2H), 3.92 – 3.90 (m, 2H), 3.90 (s, 3H), 3.88 (s, 6H), 2.90 (t, *J* = 7.32 Hz, 2H), 1.99 – 1.94 (m, 2H). ^{13}C NMR (125 MHz, $CDCl_3$) δ (ppm): 169.5, 167.9, 153.1, 141.0, 139.7, 139.2, 137.4, 132.7, 130.8, 130.6, 130.2, 129.6, 127.0, 123.9, 122.9,

107.9, 60.9, 56.3, 44.1, 26.4, 22.5. ESI-MS m/z: 486.19 $(M)^+$.

4.3.6 (*E*)-1-[(*E*)-3-(4-Bromophenyl)acryloyl]-3-(3,4,5-trimethoxybenzylidene)piperidin-2-one (5a06).

Yellow powder, 45.8% yield, m.p: 126.9-128.5 ^oC. ^1H NMR (500 MHz, $CDCl_3$) δ (ppm): 7.87 (s, 1H), 7.65 (d, *J* = 15.63 Hz, 1H), 7.59 (d, *J* = 15.62 Hz, 1H), 7.51 (d, *J* = 8.54 Hz, 1H), 7.46 (d, *J* = 8.53 Hz, 1H), 6.69 (s, 2H), 3.92-3.90 (m, 2H), 3.90 (s, 3H), 3.89 (s, 6H), 2.91 (t, *J* = 7.69 Hz, 2H), 2.00-1.94 (m, 2H). ^{13}C NMR (125 MHz, $CDCl_3$) δ (ppm): 169.6, 167.9, 153.1, 141.5, 139.6, 139.1, 134.2, 131.9, 130.8, 129.6, 124.1, 123.0, 107.7, 106.8, 60.98, 56.2, 44.1, 26.4, 22.4. ESI-MS m/z: 486.19 $(M)^+$.

4.3.7 (*E*)-1-{(*E*)-3-[2-(Trifluoromethyl)phenyl]acryloyl}-3-(3,4,5-trimethoxybenzylidene) piperidin-2-one (5a07).

Yellow powder, 34.8% yield, m.p: 101.1-102.9 ^oC. ^1H NMR (500 MHz, $CDCl_3$) δ (ppm): 8.05 (dd, *J* = 15.4, 2.1 Hz, 1H), 7.87 (s, 1H), 7.85 (d, *J* = 7.9 Hz, 1H), 7.70 (d, *J* = 7.8 Hz, 1H), 7.58 – 7.54 (m, 2H), 7.46 (t, *J* = 7.6 Hz, 1H), 6.68 (s, 2H), 3.94 – 3.89 (m, 11H), 2.93 – 2.88 (m, 2H), 1.97 (dt, *J* = 12.3, 6.2 Hz, 2H).^{13}C NMR (125 MHz, $CDCl_3$) δ (ppm): 169.1, 167.9, 153.1, 139.6 (s), 139.1 (s), 137.7 (s), 134.2, 131.9, 130.8, 129.5, 129.1, 128.2, 126.5, 126.0, 107.7, 60.9, 56.2, 44.0, 26.4, 22.4. ESI-MS m/z: 476.31 $(M)^+$.

4.3.8 (*E*)-1-[(*E*)-3-(4-Nnitrophenyl)acryloyl]-3-(3,4,5-trimethoxybenzylidene)piperidin-2-one (5a08).

Yellow powder, 34.5% yield, m.p: 180.1-182.3 ^oC. ^1H NMR (500 MHz, $CDCl_3$) δ (ppm): ^1H NMR (500 MHz, $CDCl_3$) δ 8.22 (d, *J* = 8.7 Hz, 2H), 7.86 (s, 1H), 7.71 (d, *J* = 8.7 Hz, 2H), 7.66 (s, 2H), 6.67 (s, 2H), 3.92 – 3.89 (m, 2H), 3.88 (s, 3H), 3.87 (s, 6H), 2.90 (t, *J* = 5.5 Hz, 2H), 2.00 – 1.93 (m, 2H). ^{13}C NMR (125 MHz, $CDCl_3$) δ (ppm): 169.1, 168.0, 153.1, 148.2, 141.5, 140.0, 139.1, 130.6, 129.3, 128.7, 126.7, 124.0, 107.7, 60.9, 56.2, 44.2, 26.4, 22.4. ESI-MS m/z: 453.21 $(M)^+$.

4.3.9

(*E*)-1-[(*E*)-3-(3,4-Difluorophenyl)acryloyl]-3-(3,4,5-trimethoxybenzylidene)piperidin-2-one (5a09).

Yellow powder, 39.8% yield, m.p: 149.8-151.0 ^{o}C. ^{1}H NMR (500 MHz, $CDCl_3$) δ (ppm): 7.85 (s, 1H), 7.79 (d, *J* = 15.97 Hz, 1H), 7.68 (d, *J* = 16.00 Hz, 1H), 7.35 (d, *J* = 8.07 Hz, 1H), 7.35 (s, 1H), 7.18 (t, *J* = 8.04 Hz, 1H), 6.67 (s, 2H), 3.94 (t, *J* = 5.80 Hz, 2H), 3.89 (s, 3H), 3.88 (s, 6H), 2.91 (t, *J* = 7.23 Hz, 2H), 2.00 – 1.94 (m, 2H). ^{13}C NMR (125 MHz, $CDCl_3$) δ (ppm): 169.2, 167.7, 153.0, 139.6, 139.0, 136.6, 135.9, 135.1, 132.8, 130.8, 130.5, 129.5, 129.4, 128.7, 107.7, 60.9, 56.2, 44.1, 26.4, 22.4. ESI-MS m/z: 444.19 $(M)^{+}$.

4.3.10

(*E*)-1-[(*E*)-3-(2,5-Difluorophenyl)acryloyl]-3-(3,4,5-trimethoxybenzylidene)piperidin-2-one (5a10).

Yellow powder, 36.2% yield, m.p: 134.8-136.4 ^{o}C. ^{1}H NMR (500 MHz, $CDCl_3$) δ (ppm): 7.88 (s, 1H), 7.77 (d, *J* = 15.80 Hz, 1H), 7.60 (d, *J* = 15.77 Hz, 1H), 7.36 – 7.32 (m, 1H), 7.09 – 6.99 (m, 2H), 6.69 (s, 2H), 3.94 – 3.91 (m, 2H), 3.90 (s, 3H), 3.89 (s, 6H), 2.91 (t, *J* = 7.37 Hz, 2H), 2.00 – 1.94 (m, 2H). ^{13}C NMR (125 MHz, $CDCl_3$) δ (ppm): 169.4, 167.9, 153.1, 139.8, 133.5, 130.8, 129.5, 125.9, 125.8, 117.7, 117.5, 117.2, 117.0, 114.5, 114.3, 107.8, 60.9, 56.2, 44.1, 26.4, 22.4. ESI-MS m/z: 444.19 $(M)^{+}$.

4.3.11 (*E*)-1-[(*E*)-3-(2,4-Dichlorophenyl)acryloyl]-3-(3,4,5-trimethoxybenzylidene) piperidin-2-one (5a11).

Yellow powder, 43.5% yield, m.p: 161.4-163.1 ^{o}C. ^{1}H NMR (500 MHz, $CDCl_3$) δ (ppm): 8.00 (d, *J* = 15.6 Hz, 1H), 7.86 (s, 1H), 7.67 (d, *J* = 8.48 Hz, 1H), 7.55 (d, *J* = 15.60 Hz, 1H), 7.43 (s, 1H), 7.25 (t, *J* = 6.61 Hz, 1H), 6.68 (s, 2H), 3.91 (t, *J* = 5.82 Hz, 2H), 3.89 (s, 3H), 3.88 (s, 6H), 2.90 (t, *J* = 5.63 Hz, 2H), 1.99 – 1.94 (m, 2H). ^{13}C NMR (125 MHz, CDCl3) δ (ppm): 169.2, 167.9, 153.1, 139.7, 139.2, 137.0, 135.8, 135.5, 132.1, 130.7, 129.8, 129.5, 128.6, 127.4, 125.3, 107.8, 60.9, 56.2, 44.1, 26.4, 22.4. ESI-MS m/z: 476.25 $(M)^{+}$.

4.3.12 (*E*)-1-[(*E*)-3-(2,6-Dichlorophenyl)acryloyl]-3-(3,4,5-trimethoxybenzylidene) piperidin-2-one (5a12).

Yellow powder, 46.3% yield, m.p: 124.0-125.1 ^{o}C. ^{1}H NMR (500 MHz, $CDCl_3$) δ (ppm): 7.85 (s, 1H), 7.79 (d, *J* = 15.97 Hz, 1H), 7.68 (d, *J* = 16.02 Hz, 1H), 7.35 (d, *J* = 8.15 Hz, 2H), 7.17 (t, *J* = 7.85 Hz, 1H), 6.67 (s, 2H), 3.94 (t, *J* = 5.32 Hz, 2H), 3.89 (s, 3H), 3.88 (s, 6H,), 2.90 (t, *J* = 6.16 Hz, 2H), 2.00 – 1.94 (m,2H). ^{13}C NMR (125 MHz, $CDCl_3$) δ (ppm): 169.2, 167.7, 153.1, 139.6, 139.1, 136.5, 135.9, 135.1, 132.8, 130.8, 130.5, 129.5, 129.4, 128.7, 107.8, 60.9, 56.2, 44.1, 26.4, 22.4. ESI-MS m/z: 476.18 $(M)^{+}$.

4.3.13 (*E*)-1-[(*E*)-3-(2-Chloro-6-fluorophenyl)acryloyl]-3-(3,4,5-trimethoxybenzylidene) piperidin-2-one (5a13).

Yellow powder, 45.6% yield, m.p: 129.8-131.9 ^{o}C. ^{1}H NMR (500 MHz, $CDCl_3$) δ (ppm): 7.88 (s, 1H), 7.86 (d, *J* = 15.71 Hz, 1H), 7.76 (d, *J* = 15.99 Hz, 1H), 7.26 – 7.20 (m, 2H), 7.06 – 7.01 (m, 1H), 6.68 (s, 2H), 3.93 (t, *J* = 5.84 Hz, 2H), 3.90 (s, 3H), 3.88 (s, 6H), 2.91 (t, *J* = 7.58 Hz, 2H), 2.00 – 1.94 (m, 2H). ^{13}C NMR (125 MHz, $CDCl_3$) δ (ppm): 169.9, 167.7, 153.0, 139.6, 139.0, 132.2, 130.8, 130.2, 130.1, 129.5, 129.4, 129.3, 125.8, 114.8, 114.7, 107.7, 60.9, 56.2, 44.1, 26.4, 22.4. ESI-MS m/z: 460.22 $(M)^{+}$.

4.3.14 (*E*)-1-[(*E*)-3-(2-Chloro-4-fluorophenyl)acryloyl]-3-(3,4,5-trimethoxybenzylidene) piperidin-2-one (5a14).

Yellow powder, 46.4% yield, m.p: 148.7-150.8 ^{o}C. ^{1}H NMR (500 MHz, $CDCl_3$) δ (ppm): 8.03 (d, *J* = 15.62 Hz, 1H), 7.86 (s, 1H), 7.76 – 7.72 (m, 1H), 7.53 (d, *J* = 15.59 Hz, 1H), 7.17 (d, *J* = 8.40 Hz, 1H), 7.02 – 6.98 (m, 1H), 6.68 (s, 2H), 3.93 – 3.91 (m, 2H), 3.90 (s, 3H), 3.89 (s, 6H), 2.91 (t, *J* = 7.41 Hz, 2H), 2.00 – 1.92 (m, 2H). ^{13}C NMR (125 MHz, $CDCl_3$) δ (ppm): 169.3, 167.9, 162.0, 153.1, 139.6, 137.2, 130.8, 129.6, 129.2, 129.2, 124.8, 117.4, 117.2, 114.7, 114.5, 107.8, 60.9, 56.2, 44.1, 26.4, 22.4. ESI-MS m/z: 460.01 $(M)^{+}$.

4.3.15 (*E*)-1-[(*E*)-3-(2-Fluoro-5-methoxyphenyl)acryloyl]-3-(3,4,5-trimethoxybenzylidene) piperidin-2-one (5a15).

Yellow powder, 37.5% yield, m.p: 105.7-107.4 ^{o}C. ^{1}H NMR (500 MHz, $CDCl_3$) δ (ppm): 7.87 (s, 1H), 7.81 (d, *J* = 15.77 Hz, 1H), 7.62 (d, *J* = 15.77 Hz, 1H), 7.12– 7.09 (m, 1H), 7.02 (t, *J* = 9.33 Hz, 1H), 7.88 – 7.84 (m, 1H), 6.69 (s, 2H), 3.92-3.90 (m, 2H), 3.90 (s, 3H), 3.89 (s, 6H), 3.82. ^{13}C NMR (125 MHz, $CDCl_3$) δ (ppm): 169.7, 167.8, 157.0, 155.7, 155.0, 153.1, 139.5, 135.2, 130.9, 129.7, 124.8, 117.0, 116.7, 116.5, 112.8, 107.8, 60.9, 56.2, 55.9, 44.1, 26.4, 22.51. ESI-MS m/z: 456.23 $(M)^{+}$.

4.3.16 (*E*)-1-[(*E*)-3-(2-Fluoro-4-methoxyphenyl)acryloyl]-3-(3,4,5-trimethoxybenzylidene) piperidin-2-one (5a16).

Yellow powder, 37.2% yield, m.p: 100.1-101.5 ^{o}C. ^{1}H NMR (500 MHz, $CDCl_3$) δ (ppm): 7.87 (s, 1H), 7.83 (d, *J* = 15.76 Hz, 1H), 7.58 (d, *J* = 7.67 Hz,1H), 7.57 (d, *J* = 15.89 Hz, 1H), 6.68 (s, 2H), 6.71 (d, J = 8.72 Hz, 1H), 6.64 (d, *J* = 12.35 Hz, 1H), 3.92 – 3.90 (m, 2H), 3.90 (s, 3H), 3.89 (s, 6H), 3.83 (s, 3H), 2.90 (t, *J* = 7.50 Hz, 2H), 1.98 – 1.93 (m, 2H). ^{13}C NMR (125 MHz, $CDCl_3$) δ (ppm): 169.9, 167.8, 163.4, 162.3, 153.1, 139.3, 135.6, 130.9, 129.8, 122.0, 122.0, 116.0, 110.7, 107.8, 101.8, 101.6, 60.9, 56.2, 55.7, 44.0, 26.5, 22.5. ESI-MS m/z: 456.23 $(M)^{+}$.

4.3.17 (*E*)-1-[(*E*)-3-(2-Methoxyphenyl)acryloyl]-3-(3,4,5-trimethoxybenzylidene)piperidin-2-one (5a17).

Yellow powder, 36.2% yield, m.p: 130.1-132.9 ^{o}C. ^{1}H NMR (500 MHz, $CDCl_3$) δ (ppm): 8.10 (d, *J* = 15.79 Hz, 1H), 7.86 (s, 1H), 7.64 (d, *J* = 15.76 Hz, 1H), 7.64 (d, *J* = 7.76 Hz, 1H), 7.34 (t, *J* = 8.61 Hz, 1H), 6.96 (t, *J* = 7.49 Hz, 1H), 6.91 (d, *J* = 8.28 Hz, 1H), 6.68 (s, 2H), 3.92 – 3.90 (m, 2H), 3.90 (s, 6H), 3.88 (s, 6H), 2.90 (t, *J* = 7.57 Hz, 2H), 1.98 – 1.92 (m, 2H). ^{13}C NMR (125 MHz, $CDCl_3$) δ (ppm): 170.2, 167.8, 158.3, 153.1, 139.1, 139.0, 138.4, 131.1, 131.0, 130.0, 128.5, 124.3, 122.5, 120.6, 111.1, 107.8, 60.9, 56.2, 55.5, 44.0, 26.5, 22.5. ESI-MS m/z: 438.17 $(M)^{+}$.

4.3.18 (*E*)-1-[(*E*)-3-(3-Methoxyphenyl)acryloyl]-3-(3,4,5-trimethoxybenzylidene)piperidin-2-one

(5a18).

Yellow powder, 35.3% yield, m.p: 137.6-139.0 ^{o}C. ^{1}H NMR (500 MHz, $CDCl_3$) δ (ppm): 7.87 (s, 1H), 7.70 (d, *J* = 15.59 Hz, 1H), 7.59 (d, *J* = 15.59 Hz, 1H), 7.30 (t, *J* = 7.87 Hz, 1H), 7.12 (s, 1H), 6.92 (d, *J* = 8.13 Hz, 1H), 6.69 (s, 2H), 3.92 – 3.90 (m, 2H), 3.90 (s, 3H), 3.89 (s, 6H), 3.84 (s, 3H), 2.90 (t, *J* = 7.31 Hz, 2H), 1.98 – 1.93 (m, 2H). ^{13}C NMR (125 MHz, $CDCl_3$) δ (ppm): 169.8, 167.8, 159.9, 153.1, 143.0, 139.4, 139.2, 136.6, 130.9, 129.8, 129.7, 122.7, 120.9, 115.8, 113.3, 107.8, 60.9, 56.2, 55.3, 44.0, 26.4, 22.5. ESI-MS m/z: 438.24 $(M)^{+}$.

4.3.19 (*E*)-1-[(*E*)-3-(2,4-Dimethoxyphenyl)acryloyl]-3-(3,4,5-trimethoxybenzylidene) piperidin-2-one (5a19).

Yellow powder, 32.5% yield, m.p: 143.3-145.1 ^{o}C. ^{1}H NMR (500 MHz, $CDCl_3$) δ (ppm): ^{1}H NMR (500 MHz, $CDCl_3$) δ (ppm): 8.05 (d, *J* = 15.7 Hz, 1H), 7.85 (s, 1H), 7.58 (s, 1H), 7.56 (d, *J* = 7.1 Hz, 1H), 6.68 (s, 2H), 6.49 (dd, *J* = 8.5, 2.1 Hz, 1H), 6.44 (d, *J* = 2.0 Hz, 1H), 3.88 (t, *J* = 5.1 Hz, 15H), 3.83 (s, 2H), 2.88 (t, *J* = 5.4 Hz, 2H), 2.03 – 1.86 (m, 2H). ^{13}C NMR (125 MHz, $CDCl_3$) δ (ppm): 165.2, 162.5, 157.3, 154.6, 147.8, 133.9, 133.3, 125.8, 124.8, 114.6, 112.2, 102.4, 99.9, 93.0, 55.7, 50.9, 50.2, 38.7, 21.2, 17.3. ESI-MS m/z: 468.33 $(M)^{+}$.

4.3.20 (*E*)-1-[(*E*)-3-(2,3-Dimethoxyphenyl)acryloyl]-3-(3,4,5-trimethoxybenzylidene) piperidin-2-one (5a20).

Yellow powder, 31.3% yield, m.p: 118.9-120.3 ^{o}C. ^{1}H NMR (500 MHz, $CDCl_3$) δ (ppm): 8.05 (d, *J* = 15.8 Hz, 1H), 7.86 (s, 1H), 7.63 (d, *J* = 15.7 Hz, 1H), 7.30 – 7.26 (m, 1H), 7.05 (t, *J* = 8.0 Hz, 1H), 6.93 (d, *J* = 8.1 Hz, 1H), 6.68 (s, 2H), 3.94 – 3.83 (m, 17H), 2.89 (t, *J* = 6.2 Hz, 2H), 2.00 – 1.92 (m, 2H). ^{13}C NMR (125 MHz, $CDCl_3$) δ (ppm): 170.0, 167.8, 153.1, 148.6, 139.3, 139.1, 137.6, 130.9, 129.9, 129.5, 124.0, 123.5, 119.5, 113.7, 107.8, 61.4, 60.9, 56.2, 55.9, 44.0, 26.5, 22.5. ESI-MS m/z: 468.26 $(M)^{+}$.

4.3.21 (*E*)-3-(3,4,5-Trimethoxybenzylidene)-1-[(*E*)-3-(2,4,5-trimethoxyphenyl)acryloyl] piperidin-2-one (5a21).

Yellow powder, 38.3% yield, m.p: 158.4-159.6 ^{o}C. ^{1}H NMR (500 MHz, $CDCl_3$) δ (ppm): 8.11 (d,

J = 15.7 Hz, 1H), 7.85 (s, 1H), 7.54 (d, *J* = 15.7 Hz, 1H), 7.13 (s, 1H), 6.68 (s, 2H), 6.50 (s, 1H), 3.93 (s, 3H), 3.91 – 3.87 (m, 17H), 2.91 – 2.87 (m, 2H), 1.99 – 1.92 (m, 2H). ^{13}C NMR (125 MHz, $CDCl_3$) δ (ppm): 170.3, 167.8, 154.1, 153.0, 152.1, 143.3, 139.0, 138.5, 131.0, 130.1, 119.7, 116.0, 111.0, 107.7, 97.0, 60.9, 56.5, 56.2, 56.0, 44.0, 26.5, 22.5. ESI-MS m/z: 498.22 $(M)^+$.

4.3.22 (*E*)-3-(3,4,5-Trimethoxybenzylidene)-1-[(*E*)-3-(3,4,5-trimethoxyphenyl)acryloyl] piperidin-2-one (5a22).

Yellow powder, 32.3% yield, m.p: 176.4-178.1 ^oC. ^{1}H NMR (500 MHz, DMSO-d_6) δ (ppm): δ 7.76 (s, 1H), 7.54 (d, *J* = 15.6 Hz, 1H), 7.39 (d, *J* = 15.6 Hz, 1H), 6.99 (s, 2H), 6.84 (s, 2H), 3.82 (d, *J* = 3.3 Hz, 12H), 3.79 – 3.77 (m, 2H), 3.70 (d, *J* = 2.8 Hz, 6H), 2.89 (t, *J* = 5.5 Hz, 2H), 1.90 – 1.84 (m, 2H). 13C NMR (125 MHz, $CDCl_3$) δ (ppm): 169.7, 167.9, 153.4, 153.1, 143.4, 140.1, 139.4, 139.1, 130.8, 130.8, 129.8, 121.6, 107.8, 105.6, 60.9, 56.2, 44.0, 26.4, 22.5. ESI-MS m/z: 498.22 $(M)^+$.

4.3.23 (*E*)-1-[(*E*)-3-(2,5-Dimethylphenyl)acryloyl]-3-(3,4,5-trimethoxybenzylidene)piperidin-2-one (5a23).

Yellow powder, 32.6% yield, m.p: 118.1-119.9 ^oC. ^{1}H NMR (500 MHz, $CDCl_3$) δ (ppm): 8.01 (d, *J* = 15.5 Hz, 1H), 7.88 (s, 1H), 7.51 (d, *J* = 15.5 Hz, 1H), 7.49 (s, 1H), 7.08 (s, 2H), 6.69 (s, 2H), 3.89 (d, *J* = 5.8 Hz, 9H), 2.92 – 2.88 (m, 2H), 2.42 (s, 3H), 2.33 (s, 3H), 1.97 (dt, *J* = 12.2, 6.3 Hz, 2H). ^{13}C NMR (125 MHz, $CDCl_3$) δ (ppm): 170.0, 167.9, 153.1, 141.0, 139.4, 139.0, 135.6, 134.8, 133.8, 130.9, 130.6, 129.8, 127.1, 122.9, 107.7, 60.9, 56.2, 44.0, 26.5, 22.5, 20.9, 19.3. ESI-MS m/z: 436.27 $(M)^+$.

4.3.24 2-{(*E*)-3-Oxo-3-[(*E*)-2-oxo-3-(3,4,5-trimethoxybenzylidene)piperidin-1-yl]prop-1-en-1-yl}phenyl acetate (5a24).

Yellow powder, 31.4% yield, m.p: 134.8-136.4 ^oC. ^{1}H NMR (500 MHz, $CDCl_3$) δ (ppm): 7.86 (s, 1H), 7.78 (d, *J* = 15.73 Hz, 1H), 7.74 (d, *J* = 7.77 Hz, 1H), 7.64 (d, *J* = 15.71 Hz, 1H), 7.39 (t, *J* =

8.20 Hz, 1H), 7.26 (t, *J* =7.32 Hz, 1H), 7.13 (d, *J* = 8.12 Hz,1H), 6.68 (s, 2H), 3.92 – 3.90 (m, 2H), 3.90 (s, 3H), 3.89 (s, 6H), 2.90 (t, *J* = 7.22 Hz, 2H), 2.41 (s, 3H), 1.99 – 1.93 (m, 2H). ^{13}C NMR (125 MHz, $CDCl_3$) δ (ppm): 169.5, 169.2, 167.8, 153.1, 149.4, 139.5, 139.2, 136.4, 130.8, 130.6, 129.7, 128.2, 127.9, 126.2, 124.4, 123.0, 107.8, 60.9, 56.2, 44.0, 26.4, 22.4, 21.0. ESI-MS m/z: 466.24 $(M)^+$.

4.3.25

(*E*)-1-[(*E*)-3-(2-Hydroxyphenyl)acryloyl]-3-(3,4,5-trimethoxybenzylidene)piperidin-2-one (5a25).

Yellow powder, 32.5% yield, m.p: 134.8-136.4 ^{o}C. ^{1}H NMR (500 MHz, $CDCl_3$) δ (ppm): 7.94 (d, *J* = 14.76 Hz, 1H), 7.87 (s, 1H), 7.60 (d, *J* = 15.14 Hz, 1H), 7.50 (s, 1H), 7.20 (s, 1H), 6.90 (s, 2H), 6.67 (s, 2H), 3.93 – 3.90 (m, 2H), 3.89 (s, 3H), 3.87 (s, 6H), 2.93 – 2.88 (m, 2H), 2.01 – 1.94 (m, 2H). ^{13}C NMR (125 MHz, $CDCl_3$) δ (ppm): 170.5, 168.0, 155.3, 153.1, 139.7, 139.1, 138.3, 131.0, 130.8, 129.6, 129.3, 123.6, 122.5, 120.6, 116.6, 107.9, 60.9, 56.3, 44.1, 26.5, 22.5. ESI-MS m/z: 424.24 $(M)^+$.

4.3.26

3-{(E)-3-oxo-3-[(E)-2-oxo-3-(3,4,5-trimethoxybenzylidene)piperidin-1-yl]prop-1-en-1-yl}phenyl acetate (5a26)

Yellow powder, 47.6% yield, m.p: 129.4.-131.6 ^{o}C. ^{1}H NMR (500 MHz, DMSO-d_6) δ (ppm): 7.82 (s, 1H), 7.66 (d, *J* = 12.5 Hz, 1H), 7.61 – 7.47 (m, 3H), 7.08 (s, 2H), 6.65 (s, 2H), 3.85 (s, 12H), 3.79 (s, 1H), 2.86 (s, 2H), 2.27 (s, 3H), 1.93 (s, 2H). ^{13}C NMR (125 MHz, $CDCl_3$) δ (ppm): 169.6, 167.8, 153.1, 151.8, 141.8, 139.4, 132.9, 130.8, 129.7, 129.2, 122.6, 121.9, 107.9, 60.8, 56.2, 44.0, 26.4, 22.4, 21.0. ESI-MS m/z: 465.57 $(M)^+$.

4.3.27

2-Methoxy-4-{(*E*)-3-oxo-3-[(*E*)-2-oxo-3-(3,4,5-trimethoxybenzylidene)piperidin-1-yl]prop-1-en-1-yl}phenyl acetate (5a27).

Yellow powder, 38.4% yield, m.p: 134.8-136.4 ^{o}C. ^{1}H NMR (500 MHz, $CDCl_3$) δ (ppm): 7.86 (s,

1H), 7.69 (d, *J* = 15.52 Hz, 1H), 7.52 (d, *J* = 15.58 Hz, 1H), 7.21 (d, *J* = 7.98 Hz, 1H), 7.17 (s, 1H), 7.05 (d, *J* = 8.13 Hz, 1H), 6.69 (s, 2H), 3.93 – 3.90 (m, 2H), 3.90 (s, 3H), 3.88 (s, 9H), 2.90 (t, 2H), 2.32 (s, 3H), 1.99 – 1.93 (m, 2H). ^{13}C NMR (125 MHz, $CDCl_3$) δ (ppm): 164.4, 163.5, 162.6, 147.8, 146.0, 137.2, 135.9, 134.2, 133.8, 129.0, 125.6, 124.5, 117.8, 117.3, 116.0, 106.4, 102.5, 55.7, 51.0, 50.7, 38.8, 21.2, 17.2, 15.4. ESI-MS m/z: 496.27 $(M)^+$.

4.3.28 (*E*)-1-[(*E*)-3-(4-Hydroxy-3-methoxyphenyl)acryloyl]-3-(3,4,5-trimethoxybenzylidene) piperidin-2-one (5a28).

Yellow powder, 31.6% yield, m.p: 134.8-136.4 ^{o}C. ^{1}H NMR (500 MHz, $CDCl_3$) δ (ppm): 7.86 (s, 1H), 7.70 (d, *J* = 15.51 Hz,1H), 7.50 (d, *J* = 15.50 Hz, 1H), 7.16 (d, *J* = 8.23 Hz, 1H), 7.10 (s, 1H), 6.92 (d, *J* = 8.19 Hz, 1H), 6.69 (s, 2H), 5.86 (s, 1H), 3.94 (s, 3H), 3.92 – 3.90 (m, 2H), 3.90 (s, 3H), 3.89 (s, 6H), 2.89 (t, *J* = 5.89 Hz, 2H), 1.99 – 1.93 (m, 2H). ^{13}C NMR (125 MHz, $CDCl_3$) δ (ppm): 169.9, 167.9, 153.1, 147.8, 146.7, 143.8, 139.2, 130.9, 130.0, 128.1, 127.9, 123.2, 119.8, 114.6, 109.8, 107.9, 60.9, 56.2, 56.0, 44.0, 26.4, 22.5. ESI-MS m/z: 454.20 $(M)^+$.

4.3.29

2-Methoxy-5-{(*E*)-3-oxo-3-[(*E*)-2-oxo-3-(3,4,5-trimethoxybenzylidene)piperidin-1-yl]prop-1-en-1-yl}phenyl acetate (5a29).

Yellow powder, 38.3% yield, m.p: 134.8-136.4 ^{o}C. ^{1}H NMR (500 MHz, $CDCl_3$) δ (ppm): 7.86 (s, 1H), 7.68 (d, *J* = 15.51 Hz, 1H), 7.51 (d, *J* = 15.53 Hz, 1H), 7.43 (d, *J* = 8.32 Hz, 1H), 7.35 (s, 1H), 6.95 (d, *J* = 8.44 Hz, 1H), 6.69 (s, 2H), 3.91 – 3.89 (m, 2H), 3.90 (s, 3H), 3.89 (s, 6H), 3.86 (s, 3H), 2.89 (s, 2H), 2.32 (s, 3H), 1.99 – 1.92 (m, 2H). ^{13}C NMR (125 MHz, $CDCl_3$) δ (ppm): 169.6, 168.6, 167.8, 153.1, 142.3, 142.2, 140.1, 139.3, 130.9, 129.9, 128.5, 127.9, 122.0, 120.9, 112.2, 107.9, 60.9, 56.2, 55.9, 44.0, 26.4, 22.5, 20.5. ESI-MS m/z: 496.27 $(M)^+$.

4.4 Cells and Reagents

The final concentration of DMSO in assays did not exceed 0.1%. All other reagents not mentioned were obtained from Sigma unless otherwise specified. Mouse peritoneal macrophages (MPMs) were prepared as described previously [31]. Briefly, ICR mice of 20–25 g were

intraperitoneally injected with 6% thioglycollate solution [beef extract (0.3 g), tryptone (1 g), sodium chloride (0.5 g) and soluble starch (6 g) in 100 mL water]. 3 days later, the mice were sacrificed. The peritoneal cavity was washed with 8 mL of PBS, and centrifuged at 4 °C, 1000 rpm. The supernatant was discarded, the precipitate resuspended with RPMI-1640 (Gibco/BRL life Technologies, Eggenstein, Germany) containing 10% (v/v) FBS (Hyclone, Logan, UT, USA), 100 U/mL penicillin G and 100 mg/mL streptomycin. Cells were incubated at 37 °C under a 5% CO_2 atmosphere.

4.5 Immunofluorescence and immunoblotting

Raw 264.7 cells were seeded into 6-well plates and pretreated with compounds for 0.5 hour, followed by incubation with LPS for another 40 minutes. Thereafter, cells were fixed and permeabilized with 4% paraformaldehyde and 100% methanol, respectively. Cells were washed twice with PBS containing 1% BSA, then incubated with primary antibodies of P65 (1:200) at 4 °C overnight. Samples were subsequently incubated with PE-conjugated secondary antibodies (1:200) for 2 hours. Finally, cells were counterstained with DAPI, and viewed with a Nikon fluorescence microscope (Nikon, Japan).

For immunoblotting assays, cells or lung tissues (weight of 30–50 mg) were lysed (Boster Biological Technology, USA). Protein concentration was measured using a Bio-Rad protein assay kit (Bio-rad, USA). Samples were loaded and separated in 10% or 12% SDS-PAGE gels. The gel was electro-transferred to a nitrocellulose membrane, and blocked in Tris-buffered saline at pH 7.6 containing 0.05% Tween 20 and 5% non-fat milk. Specific antibodies were incubated for biomarkers. Immuno-reactive bands were detected by incubating with secondary antibodies conjugated with horseradish peroxidase, and visualized using enhanced chemiluminescence reagents (Bio-Rad, Hercules, CA).

P-P38, P38, P-ERK, ERK, P65, IκBα and GAPDH antibodies were purchased from Cell Signaling Technology (Danvers, MA, USA). TNF-α antibodies were obtained from Abcam (Abcam, USA). Secondary antibodies were purchased from Yeasen Biotechnology (Shanghai, China).

4.6 Determination of concentrations of TNF-α and IL-6

TNF-α and IL-6 concentrations in culture medium or animal samples were determined by ELISA according to the manufacturer's instructions (Bioscience, San Diego, CA). The amount of TNF-α or IL-6 was normalized to the protein concentration of each sample.

4.7 Real-time quantitative PCR

Total RNA was extracted using TRIZOL (Life Technologies, Carlsbad, CA). Reverse transcription and quantitative PCR (RT-qPCR) were set up using M-MLV Platinum RT-qPCR Kit (Life Technologies). Real-time qPCR was carried out on an Eppendorf Realplex 4 instrument (Eppendorf, Hamburg, Germany). Primers for genes (i.e. TNF-α, IL-6 and β-actin) were obtained from Life Technologies. The primer sequences used are shown in Table 2. The relative amount of each gene was normalized to β-actin.

Table 2. Primers used for real-time qPCR assay

Gene	Species	Forward (5'-3')	Reverse (5'-3')
TNF-α	Mouse	TGATCCGCGACGTGGAA	ACCGCCTGGAGTTCTGGAA
IL-6	Mouse	GAGGATACCACTCCCAACAGACC	AAGTGCATCATCGTTGTTCATACA
β-actin	Mouse	CCGTGAAAAGATGACCCAGA	TACGACCAGAGGCATACAG

4.8 Mouse models

Male C57BL/6 mice of 20–25 g were obtained from the Animal Centre of Wenzhou Medical University (Wenzhou, China). Mice were housed at constant room temperature with a 12:12 h light–dark cycle, fed a standard rodent diet and water, and acclimatized to the laboratory for at least 3 days before use. All animal care and experimental procedures were approved by the Wenzhou Medical College Animal Policy and Welfare Committee.

LPS-induced ALI. The mice were randomly divided into groups as follows: control (eight mice received vehicle of 0.9% saline), LPS (eight mice received LPS alone), curcumin, **5a27** or **5a28** (each of the three compounds was administered to a group of eight mice at 10 mg/kg). The active

compounds were given daily via intraperitoneal injection consecutively for one week. The mice were euthanized with chloral hydrate 6 hours after intratracheal injection of LPS at 5 mg/kg. Broncho alveolar lavage fluid (BALF), blood and lung tissues were collected for further analysis.

4.9 Histomorphological and immunohistochemical examination

Lung tissues were routinely fixed and embedded in paraffin. Paraffin blocks were sectioned into slices of 5 μm thick. Thereafter, the slices were stained with Hematoxylin and Eosin (H&E assay kit, Beyotime, Shanghai, China).

For immunohistochemistry, rehydrated slices were subjected to antigen retrieval in 0.01 mol/L citrate buffer (pH 6.0) by microwaving, and then placing in 3% hydrogen peroxide in methanol at room temperature for 30 min. Sections were incubated with primary antibodies at 4 °C overnight, followed by secondary antibodies (1:200; Santa Cruz, USA). The slices were visualized by 3,3-diaminobenzidine (DAB) (ZSGB-Bio, Beijing, China), counterstained with hematoxylin, and viewed under the microscope (Nikon, Japan).

4.10 Pharmacokinetic study of 5a27

Male SD rats, weight 250 ± 20 g, were starved overnight before the experiment. Tap water was available *ad libitum*. Intragastric or intravenously administration of 5a27 with the dose of 20 mg/kg, 5 mg/kg respectively (n = 5). Blood samples from tail were collected 0.083, 0.25, 0.5, 1, 2, 4, 6, 9, 12, 24 hours after dosing. They were centrifuged at 12000 rpm for 10 minutes. Remove supernatants to 1.5 mL tube and add 2-fold volume of acetonitrile. The mixtures were vortexed and centrifuged at 12000 rpm for 10 minutes. The supernatants were analyzed by UHPLC-MS/MS. The pharmacokinetic parameters were determined by using DAS software (Version 3.0).

4.11 Statistical analysis

All data were shown as means ± SEM, by averaging values from three independent experiments. Statistical analyses were performed using GraphPad Pro. Prism 5.0 (GraphPad, San Diego, CA). One-way ANOVA followed by multiple comparisons test with Bonferroni correction were used to analyze the differences between sets of data.

Acknowledgement

Financial support was provided by the National Natural Science Funding of China (81773579, 81803600), Zhejiang Natural Science Funding (LY17B020008), and the Wenzhou Public Welfare Science and Technology Project (2018Y0465). We also thank Amy Tong from Liwen Bianji, Edanz Editing China (www.liwenbianji.cn/ac), for editing the English text of a draft of this manuscript.

Reference

[1] G.D. Rubenfeld, E. Caldwell, E. Peabody, J. Weaver, D.P. Martin, M. Neff, E.J. Stern, L.D. Hudson, Incidence and outcomes of acute lung injury, N. Engl. J. Med. 353 (2005) 1685-1693.

[2] G.A. Schmidt, Managing Acute Lung Injury, Clin. Chest Med. 37 (2016) 647-658.

[3] D. Impellizzeri, G. Bruschetta, E. Esposito, S. Cuzzocrea, Emerging drugs for acute lung injury, Expert Opin. Emerg. Drugs, 20 (2015) 75-89.

[4] R.B. Goodman, J. Pugin, J.S. Lee, M.A. Matthay, Cytokine-mediated inflammation in acute lung injury, Cytokine Growth Factor Rev. 14 (2003) 523-535.

[5] Y. Butt, A. Kurdowska, T.C. Allen, Acute Lung Injury: A Clinical and Molecular Review, Arch. Pathol. Lab. Med. 140 (2016) 345-350.

[6] D. Dreyfuss, J.D. Ricard, Acute lung injury and bacterial infection, Clin. Chest Med. 26 (2005) 105-112.

[7] M. Chopra, J.S. Reuben, A.C. Sharma, Acute lung injury:apoptosis and signaling mechanisms, Exp. Biol. Med. (Maywood) 234 (2009) 361-371.

[8] D.J. Newman, G.M. Cragg, Natural Products as Sources of New Drugs from 1981 to 2014, J.

Nat. Prod. 79 (2016) 629-661.

[9] IP.S. Fernando, J.W. Nah, Y.J. Jeon, Potential anti-inflammatory natural products from marine algae, Environ. Toxicol. Pharmacol. 48 (2016) 22-30.

[10] P. Basnet, N. Skalko-Basnet, Curcumin: an anti-inflammatory molecule from a curry spice on the path to cancer treatment, Molecules 16 (2011) 4567-4598.

[11] R.L. Edwards, P.B. Luis, P.V. Varuzza, A.I. Joseph, S.H. Presley, R. Chaturvedi, C. Schneider, The anti-inflammatory activity of curcumin is mediated by its oxidative metabolites, J. Biol. Chem. 292 (2017) 21243-21252.

[12] H.P. Zhu, T.T. Xu, C.Y. Qiu, B.B. Wu, Y.L. Zhang, L.F. Chen, Q.Q. Xia, C.L. Li, B. Zhou, Z.G. Liu, G. Liang, Synthesis and optimization of novel allylated mono-carbonyl analogs of curcumin (MACs) act as potent anti-inflammatory agents against LPS-induced acute lung injury (ALI) in rats, Eur. J. Med. Chem. 121 (2016) 181-193.

[13] Y. Fazal, S.N. Fatima, S.M. Shahid, T. Mahboob, Effects of curcumin on angiotensin-converting enzyme gene expression, oxidative stress and anti-oxidant status in thioacetamide-induced hepatotoxicity, J Renin Angiotensin Aldosterone Syst. 16 (2015) 1046-1051.

[14] M. Pisano, G. Pagnan, M.A. Dettori, S. Cossu, I. Caffa, I. Sassu, L. Emionite, D. Fabbri, M. Cilli, F. Pastorino, G. Palmieri, G. Delogu, M. Ponzoni, C. Rozzo, Enhanced anti-tumor activity of a new curcumin-related compound against melanoma and neuroblastoma cells, Mol. Cancer 9 (2010) 137.

[15] X.P. Wang, Q.X. Wang, H.P. Lin, N. Chang, Anti-tumor bioactivities of curcumin on mice loaded with gastric carcinoma, Food Funct. 8 (2017) 3319-3326.

[16] S. Peng, Z. Li, L. Zou, W. Liu, C. Liu, D.J. McClements, Improving curcumin solubility and bioavailability by encapsulation in saponin-coated curcumin nanoparticles prepared using a simple pH-driven loading method, Food Funct. 9 (2018) 1829-1839.

[17] M.C. Bonferoni, S. Rossi, G. Sandri, F. Ferrari, Nanoparticle formulations to enhance tumor targeting of poorly soluble polyphenols with potential anticancer properties, Semin. Cancer Biol. 46 (2017) 205-214.

[18] C. Zhao, Z. Liu, G. Liang, Promising curcumin-based drug design: mono-carbonyl analogues of curcumin (MACs), Curr. Pharm. Des.,19 (2013) 2114-2135.

[19] C. Schneider, O.N. Gordon, R.L. Edwards, P.B. Luis, Degradation of Curcumin: From Mechanism to Biological Implications, J. Agric. Food Chem., 63 (2015) 7606-7614.

[20] K.I. Priyadarsini, The chemistry of curcumin: from extraction to therapeutic agent, Molecules 19 (2014) 20091-20112.

[21] Y.J. Wang, M.H. Pan, A.L. Cheng, L.I. Lin, Y.S. Ho, C.Y. Hsieh, J.K. Lin, Stability of curcumin in buffer solutions and characterization of its degradation products, J. Pharm. Biomed. Anal. 15 (1997) 1867-1876.

[22] P.T. Yu, L.L. Dong, Y.L. Zhang, W.B. Chen, S.M. Xu, Z. Wang, X.O. Shan, J.M. Zhou, Z.G. Liu, G. Liang, Design, synthesis and biological activity of novel asymmetric C66 analogs as anti-inflammatory agents for the treatment of acute lung injury, Eur. J. Med. Chem. 94 (2015) 436-446.

[23] G. Liang, S. Yang, L. Jiang, Y. Zhao, L. Shao, J. Xiao, F. Ye, Y. Li, X. Li, Synthesis and anti-bacterial properties of mono-carbonyl analogues of curcumin, Chem. Pharm. Bull (Tokyo). 56 (2008): 162-167.

[24] D.J. Son, S.Y. Kim, S.S. Han, C.W. Kim, S. Kumar, B.S. Park, S.E. Lee, Y.P. Yun, H. Jo, Y.H. Park, Piperlongumine inhibits atherosclerotic plaque formation and vascular smooth muscle cell proliferation by suppressing PDGF receptor signaling, Biochem. Biophys. Res. Commun. 427 (2012) 349-354.

[25] N. Kim, J. Do, J.S. Bae, H.K. Jin, J.H. Kim, K.S. Inn, M.S. Oh, J.K. Lee, Piperlongumine inhibits neuroinflammation via regulating NF-kappaB signaling pathways in lipopolysaccharide-stimulated BV2 microglia cells, J. Pharmacol. Sci. 137 (2018) 195-201.

[26] F. de Faria Ghetti, D.G. Oliveira, J.M. de Oliveira, L. de Castro Ferreira, D.E. Cesar, A.P.B. Moreira, Influence of gut microbiota on the development and progression of nonalcoholic steatohepatitis, Eur. J. Nutr. 57 (2018) 861-876.

[27] Z.G. Liu, L.G. Tang, H.P. Zhu, T.T. Xu, C.Y. Qiu, S.Q. Zheng, Y.G. Gu, J.P. Feng, Y.L. Zhang, G. Liang, Design, Synthesis, and Structure-Activity Relationship Study of Novel Indole-2-carboxamide Derivatives as Anti-inflammatory Agents for the Treatment of Sepsis, J. Med. Chem. 59 (2016) 4637-4650.

[28] L.J. Cross, M.A. Matthay, Biomarkers in acute lung injury: insights into the pathogenesis of acute lung injury, Crit. Care Clin. 27 (2011) 355-377.

[29] G. Chen, Y. Zhang, X. Liu, Q. Fang, Z. Wang, L. Fu, Z. Liu, Y. Wang, Y. Zhao, X. Li, G. Liang, Discovery of a new inhibitor of myeloid differentiation 2 from cinnamamide derivatives with anti-Inflammatory activity in sepsis and acute lung injury, J. Med. Chem. 59 (2016) 2436-2451.

[30] K.Y. Yang, L.C. Lin, T.Y. Tseng, S.C. Wang, T.H. Tsai, Oral bioavailability of curcumin in rat and the herbal analysis from Curcuma longa by LC-MS/MS, J. Chromatogr. B Analyt.

Technol. Biomed. Life Sci. 853(2007) 183-189.

[31] O.J. Broom, B. Widjaya, J. Troelsen, J. Olsen, O.H. Nielsen, Mitogen activated protein kinases: a role in inflammatory bowel disease?, Clin. Exp. Immunol. 158 (2009) 272-280.

Figure Legends

Table 1. The pharmacokinetic parameters of 5a27 in rats.

Figure 1. Structures of curcumin, C03, piperlongumine and the conceptual design of DACs.

Figure 2. Active DACs effectively inhibit the production of proinflammatory cytokines without cytotoxicity. A–B) MPMs were pretreated with compounds (10 μM) for 0.5 hour, followed by incubation with LPS for another 24 hours. Harvest conditions and determination of concentrations of TNF-α and IL-6 using ELISA assay are described in "Methods". **C**) MPMs were treated with compounds for 24 h. Cell viability was measured by MTT assay, and presented as a percentage of that in the control (DMSO). The data were shown as mean ± SEM, n=3. **, $p < 0.01$; ***, $p < 0.001$, *vs.* LPS.

Figure 3. Active DACs dose-dependently inhibited the production of TNF-α and IL-6 in activated MPMs. MPMs were pretreated with the indicated doses of **5a27** and **5a28.** Cells were incubated with LPS for 24 hours. ELISA assay was employed to detect the release of TNF-α and IL-6 in the culture medium. The data were displayed as mean ± SEM, n=3. ***, $p < 0.001$, *vs.* LPS.

Figure 4. The stability and bioavailability of active DACs were improved compared to curcumin. UV-visible absorption spectra of curcumin (A), **5a27** (B) and **5a28** (C) in phosphate buffer (pH 7.4). D) **5a27** was administrated to rats through orally and intravenously, n= 5. The blood samples were collected from tail. After samples preparation, the concentration of **5a27** was determined by UHPLC-MS/MS. The time-concentration curve was plotted.

Figure 5. 5a27 and 5a28 potently suppressed LPS-induced activation of macrophages through blocking MAPK signaling and NF-kB activation. A) RAW 264.7 mouse macrophages were pretreated with compounds for 0.5 hour, followed by incubation with LPS for 30 min. The

cell lysates were subjected to immunoblotting assay for p-p38, p38, p-erk, erk, ikB and GAPDH. The representative images were shown. **B**) RAW 264.7 cells were pretreated with compounds for 0.5 hour. Thereafter, cells were stimulated with LPS for 45 minutes. Immunofluorescence assay was used to detect p65 (Red), with nuclei stained with DAPI (Blue). **C-G**) RAW 264.7 cells were activated as aforementioned. Total RNA was extracted and subjected to real time-qPCR for TNF-α, IL-6, IL-1β, ICAM-1 and VCAM-1. The values were normalized to actin, and compared with the LPS group. *, $p < 0.05$; **, $p < 0.01$; ***, $p < 0.001$, *vs.* LPS.

Figure 6. Active DACs improved LPS-induced ALI by inhibiting inflammation. C57BL/6 mice were pretreated with curcumin (cur), **5a27** and **5a28** at 10 mg/kg for 30 min, followed by intra-tracheal injection of LPS at 5 mg/kg. 6 hours later, BALF, serum and lung samples were collected and analyzed. The wet/dry ratio of lung (**A**), total cell count (**B**) and neutrophil count (**C**) in BALF were determined. **D**) Lung tissues were subjected to immunohistochemical assays. H&E, LY-6G and F4/80 were detected. **E-F**) Concentrations of TNF-α and IL-6 were determined by ELISA assay in serum and BALF samples. Data were shown as mean ± SEM, n=6. *, $p < 0.05$; **, $p < 0.01$ *vs.* LPS alone.

Figure 7. Active DACs significantly suppressed the production of inflammatory cytokines and adhesion factors. Lung samples were collected and subjected to real-time Q-PCR assay. mRNA expressions of TNF-α (**A**), IL-6 (**B**), IL-1β (**C**), VCAM-1 (**D**) and ICAM-1 (**E**) were determined. Data were shown as mean ± SEM. *, $p < 0.05$; **, $p < 0.01$; ***, $p < 0.001$, *vs.* LPS.

Scheme 1. Synthetic route of di-carbonyl analogs of curcumin (DACs) 5a01-5a29. Reagents and conditions: (a) Oxalyl chloride, DMF, CH_2Cl_2, rt, 5h; (b) *tert*-butyl 2-oxopiperidine-1-carboxylate, NaH, THF, 0 ^{o}C-rt, 4h; (c) *n*-BuLi, THF, -78 ^{o}C, 4h; (d) 20% (w/v) $NaHCO_3$, MeOH/THF, rt, overnight.

Table 1.

Administration	AUC(0-t) (μg/L*h)	AUC(0-∞) (μg/L*h)	MRT(0-t) (h)	MRT(0-∞) (h)	t1/2 (h)	Tmax (h)	CLz/F (L/h/kg)	Vz/F (L/kg)	Cmax (μg/L)
p.o 50mg/kg	231.2 ± 332.7	325.6 ± 310.7	7.8 ± 4.5	12.3 ± 9.5	6.7 ± 7.7	3.3 ± 4.2	5062.6 ± 5506.5	827.1 ± 1314.3	113.3 ± 152.4
i.v 5mg/kg	34.4 ± 41.7	122.4 ± 74.5	11.3 ± 3.3	19.9 ± 7.5	0.2 ± 0.1	0.1 ± 0.1	404.4 ± 113.7	59.5 ± 47.9	16.4 ± 19.7

Figure 1

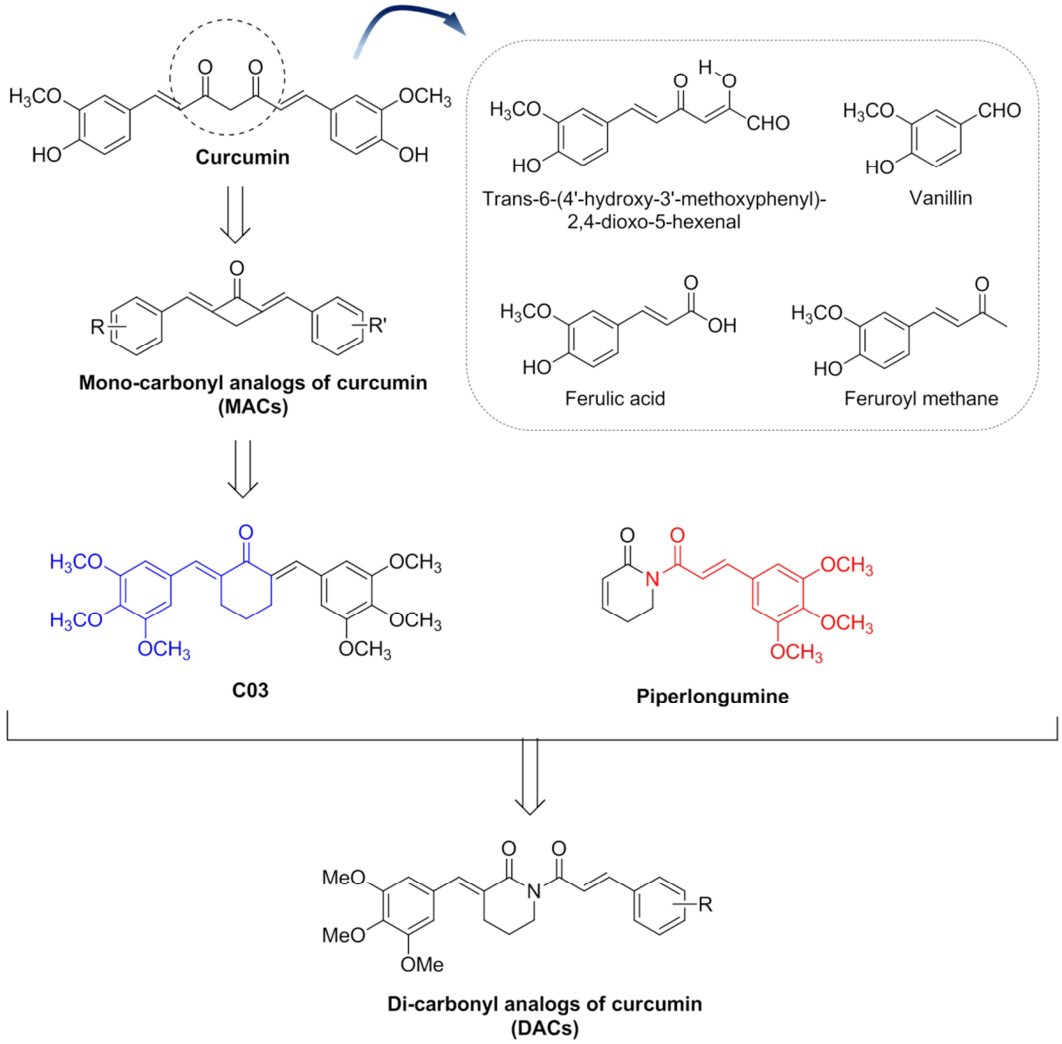

Figure 2

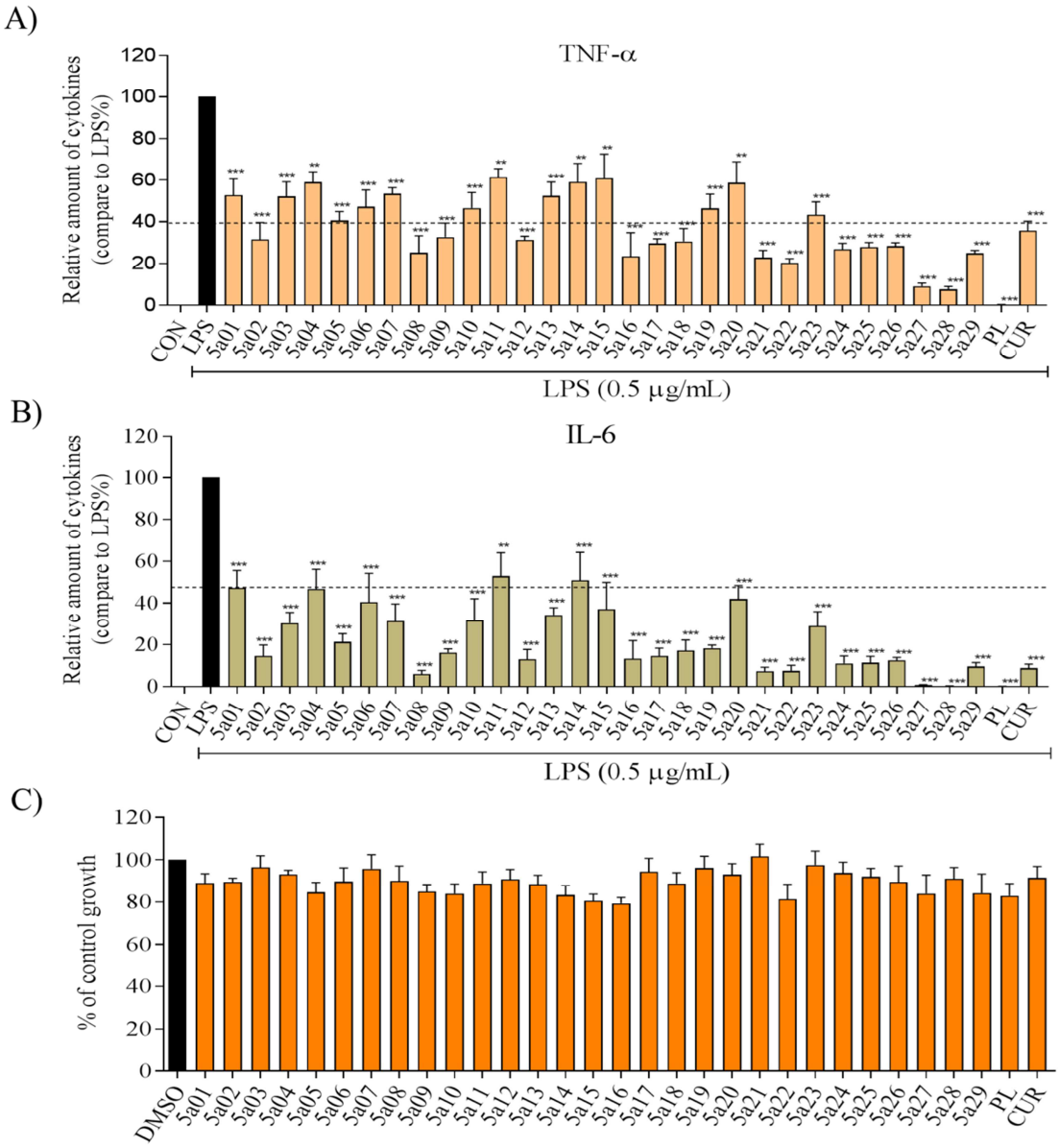
A)
TNF-α
Relative amount of cytokines (compare to LPS%)
120
100
80
60
40
20
0
CON
LPS
5a01
5a02
5a03
5a04
5a05
5a06
5a07
5a08
5a09
5a10
5a11
5a12
5a13
5a14
5a15
5a16
5a17
5a18
5a19
5a20
5a21
5a22
5a23
5a24
5a25
5a26
5a27
5a28
5a29
PL
CUR
LPS (0.5 μg/mL)
B)
IL-6
Relative amount of cytokines (compare to LPS%)
120
100
80
60
40
20
0
CON
LPS
5a01
5a02
5a03
5a04
5a05
5a06
5a07
5a08
5a09
5a10
5a11
5a12
5a13
5a14
5a15
5a16
5a17
5a18
5a19
5a20
5a21
5a22
5a23
5a24
5a25
5a26
5a27
5a28
5a29
PL
CUR
LPS (0.5 μg/mL)
C)
% of control growth
120
100
80
60
40
20
0
DMSO
5a01
5a02
5a03
5a04
5a05
5a06
5a07
5a08
5a09
5a10
5a11
5a12
5a13
5a14
5a15
5a16
5a17
5a18
5a19
5a20
5a21
5a22
5a23
5a24
5a25
5a26
5a27
5a28
5a29
PL
CUR

Figure 3

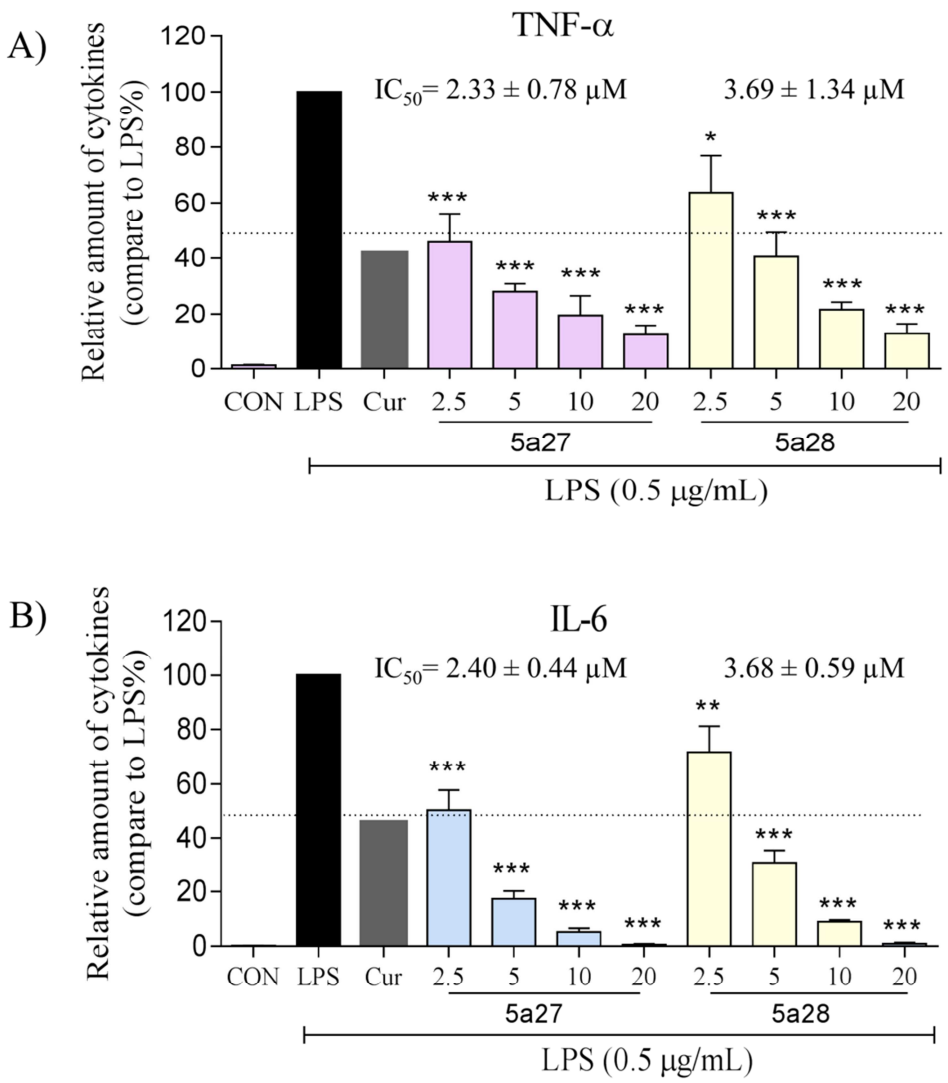
A)
TNF-α
IC50= 2.33 ± 0.78 μM
3.69 ± 1.34 μM
Relative amount of cytokines (compare to LPS%)
120
100
80
60
40
20
0
CON LPS Cur 2.5 5 10 20 2.5 5 10 20
5a27
5a28
LPS (0.5 μg/mL)
B)
IL-6
IC50= 2.40 ± 0.44 μM
3.68 ± 0.59 μM
Relative amount of cytokines (compare to LPS%)
CON LPS Cur 2.5 5 10 20 2.5 5 10 20
5a27
5a28
LPS (0.5 μg/mL)

Figure 4

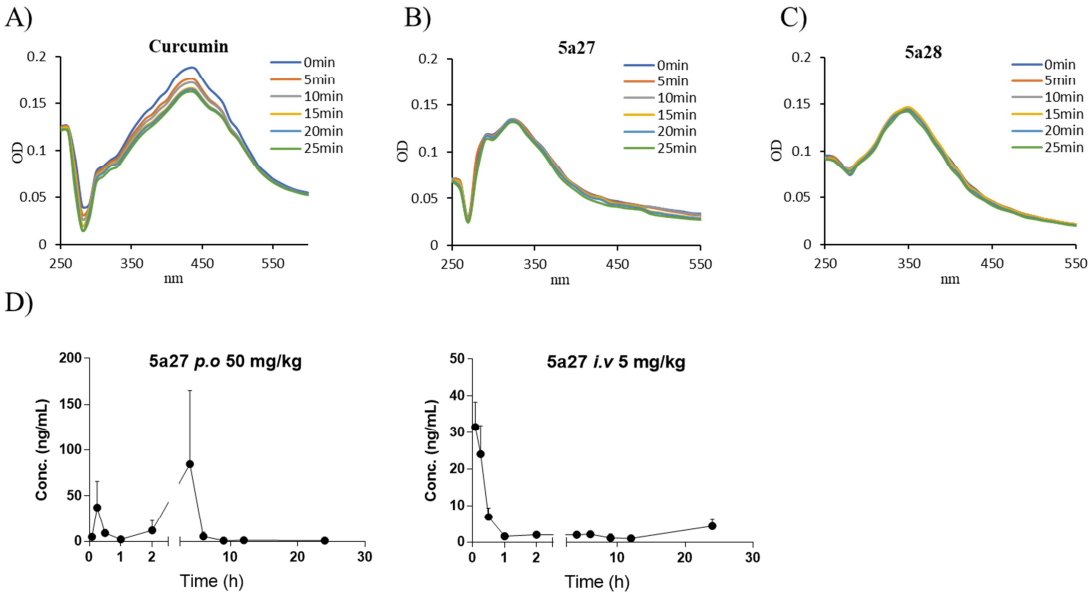

Figure 5

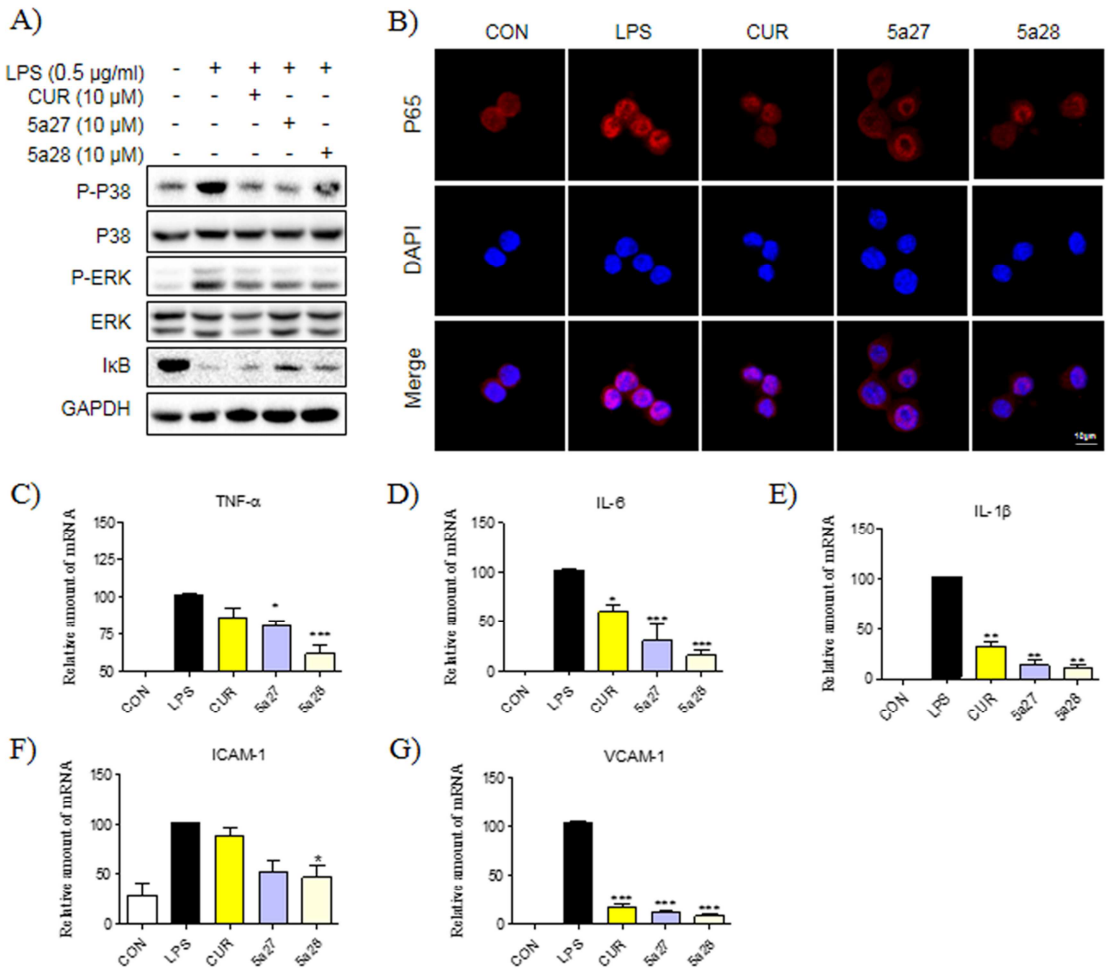

Figure 6

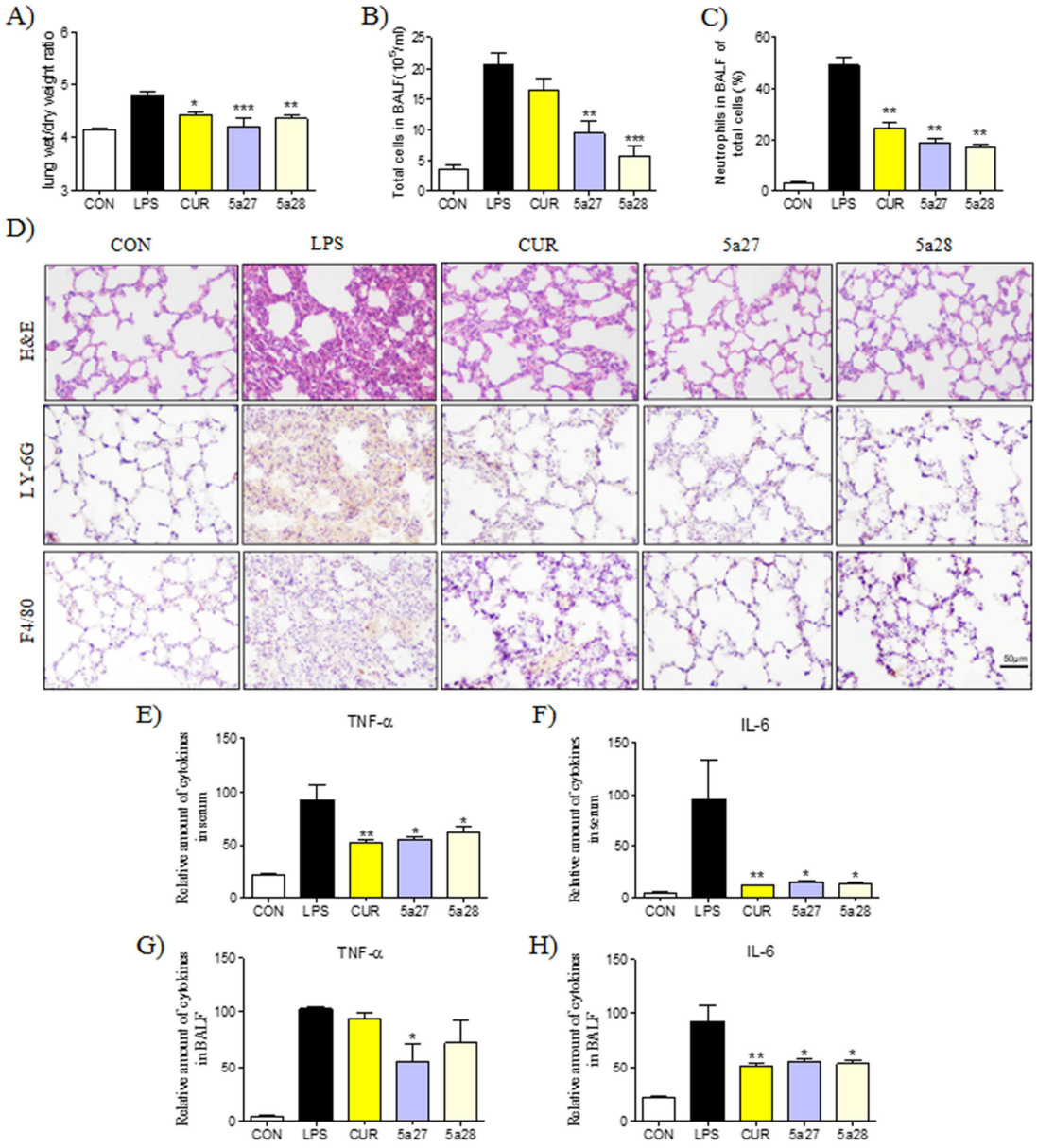
A)
lung wet/dry weight ratio
CON
LPS
CUR
5a27
5a28
B)
Total cells in BALF (10^5/ml)
C)
Neutrophils in BALF of total cells (%)
D)
H&E
LY-6G
F4/80
50μm
E)
TNF-α
Relative amount of cytokines in serum
F)
IL-6
G)
Relative amount of cytokines in BALF
H)

Figure 7

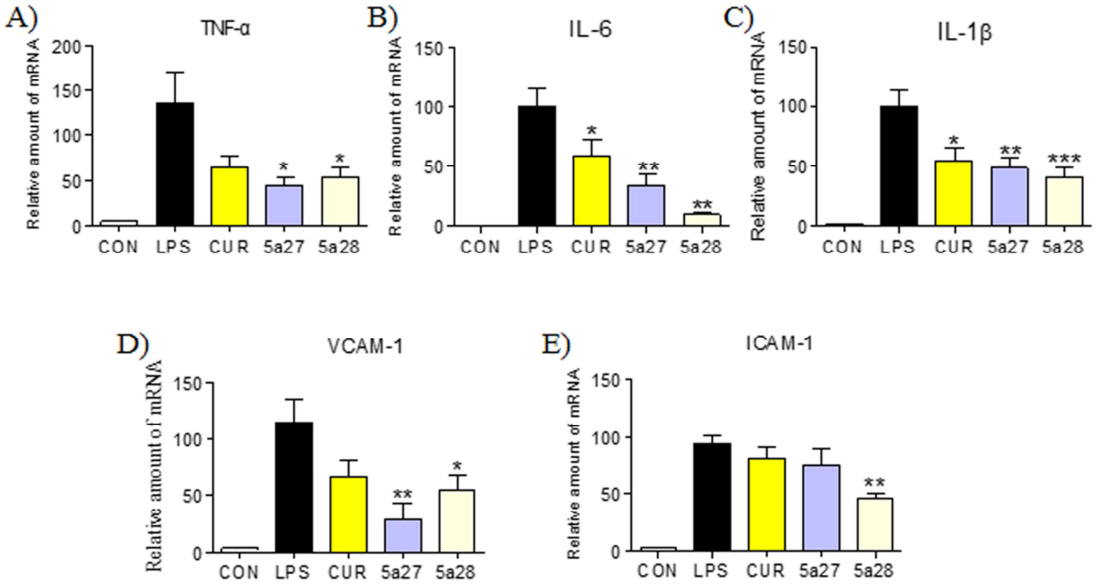

Scheme 1

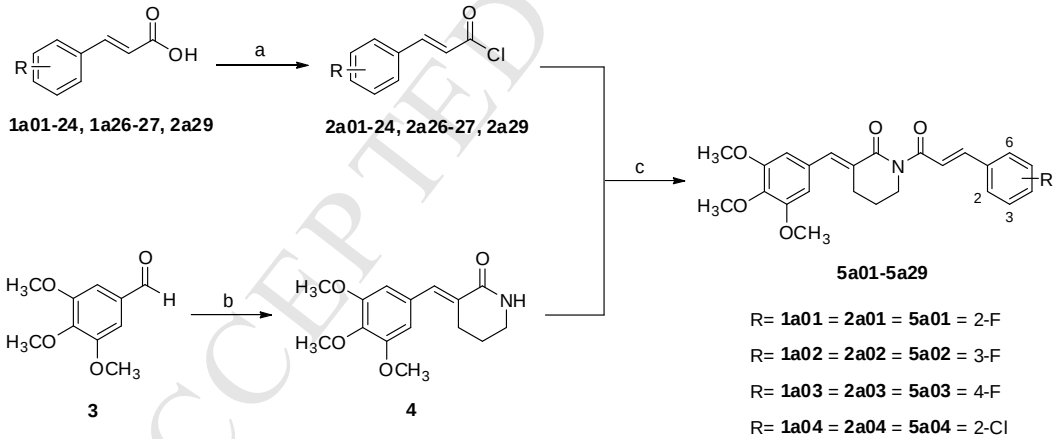

R= **1a01** = **2a01** = **5a01** = 2-F

R= **1a02** = **2a02** = **5a02** = 3-F

R= **1a03** = **2a03** = **5a03** = 4-F

R= **1a04** = **2a04** = **5a04** = 2-Cl

R= **1a05** = **2a05** = **5a05** = 3-Br

R= **1a06** = **2a06** = **5a06** = 4-Br

R= **1a07** = **2a07** = **5a07** = 2-CF_3

R= **1a08** = **2a08** = **5a08** = 4-NO_2

R= **1a09** = **2a09** = **5a09** = 3,4-F

R= **1a10** = **2a10** = **5a10** = 2,5-F

R= **1a11** = **2a11** = **5a11** = 2,4-Cl

R= **1a12** = **2a12** = **5a12** = 2,6-Cl

R= **1a13** = **2a13** = **5a13** = 2-F, 6-Cl

R= **1a14** = **2a14** = **5a14** = 2-Cl, 4-F

R= **1a15** = **2a15** = **5a15** = 2-F, 5-OMe

R= **1a16** = **2a16** = **5a16** = 2-F, 4-OMe

R= **1a17** = **2a17** = **5a17** = 2-OMe

R= **1a18** = **2a18** = **5a18** = 3-OMe

R= **1a19** = **2a19** = **5a19** = 2,4-OMe

R= **1a20** = **2a20** = **5a20** = 2,3-OMe

R= **1a21** = **2a21** = **5a21** = 2,4,5-OMe

R= **1a22** = **2a22** = **5a22** = 3,4,5-OMe

R= **1a23** = **2a23** = **5a23** = 2,5-Me

R= **1a24** = **2a24** = 2-OAc = **5a24**

d

R= **5a25** = 2-OH

R= **1a26** = **2a26** = **5a26** = 4-OAc

R= **1a27** = **2a27** = 3-OMe, 4-OAc = **5a27**

d

R= **5a28** = 3-OMe, 4-OH

R= **1a29** = **2a29** = **5a29** = 3-OAc, 4-OMe

Highlights

- 29 novel di-carbonyl analogs of curcumin (DACs) were synthesized and evaluated for anti-inflammatory activity.
- Active DACs **5a27** and **5a28** exhibited better structural stability and anti-inflammatory activity than curcumin.
- Compound **5a27** and **5a28** could be lead compounds as an ALI therapeutic agent.